iScience

CellPress

Article

Allosteric Regulation of Hsp90α's Activity by Small Molecules Targeting the Middle Domain of the Chaperone

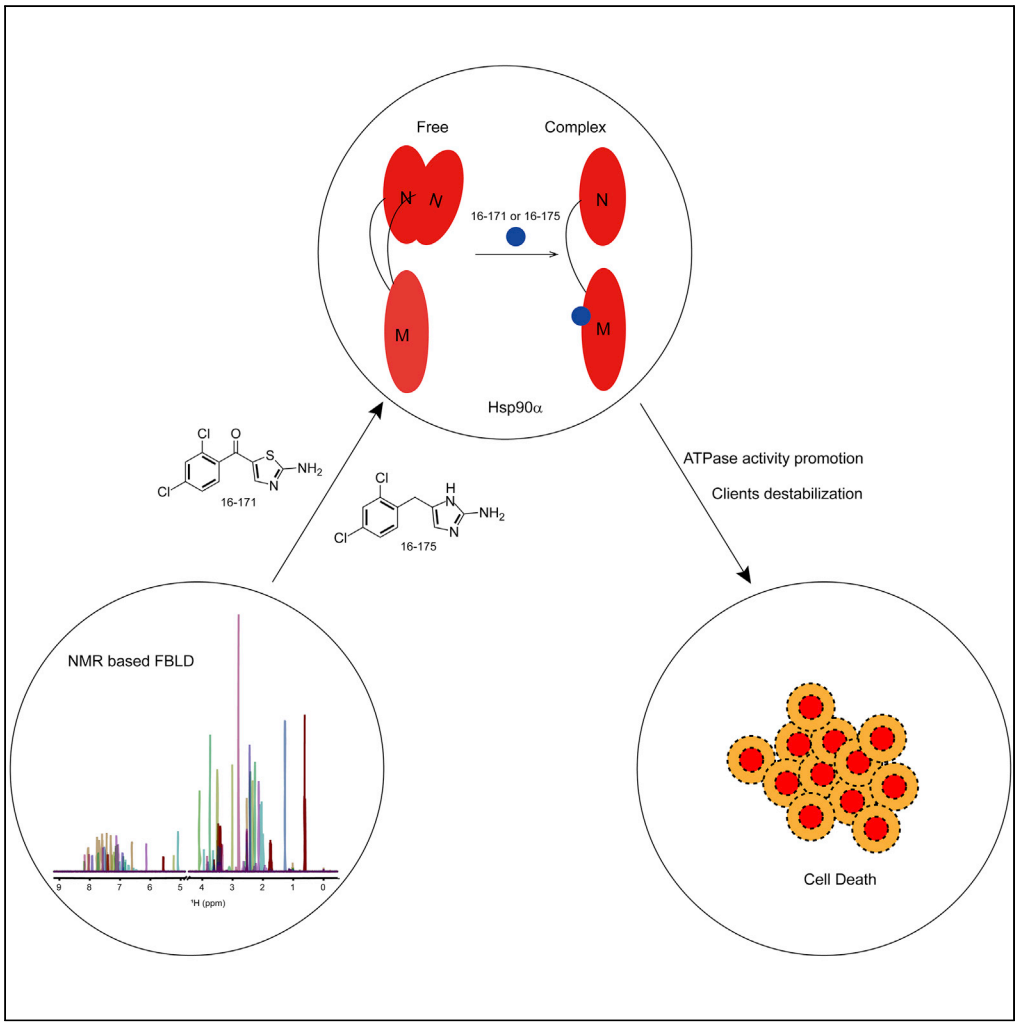

Chen Zhou, Chi Zhang, Hongwen Zhu, ..., Yechun Xu, Ao Zhang, Naixia Zhang

ycxu@simm.ac.cn (Y.X.)
aozhang@simm.ac.cn (A.Z.)
nxzhang@simm.ac.cn (N.Z.)

HIGHLIGHTS

Allosteric modulators targeting Hsp90α's middle domain were developed for the first time

Key elements in Hsp90M for the recognition of allosteric modulators were identified

Compound SOMCL-16-175 promotes Hsp90α's ATPase activity and reduces cell viability

SOMCL-16-175 destabilizes Hsp90's clients without triggering heat shock response

DATA AND CODE AVAILABILITY

6KSQ

Zhou et al., iScience *23*, 100857
February 21, 2020
https://doi.org/10.1016/j.isci.2020.100857

iScience

CellPress

Article

Allosteric Regulation of Hsp90α's Activity by Small Molecules Targeting the Middle Domain of the Chaperone

Chen Zhou,[1,5] Chi Zhang,[2,5] Hongwen Zhu,[1,2,5] Zhijun Liu,[3] Haixia Su,[2,4] Xianglei Zhang,[2,4] Tingting Chen,[2,4] Yan Zhong,[1,4] Huifang Hu,[1,4] Muya Xiong,[2,4] Hu Zhou,[2,4] Yechun Xu,[2,4,*] Ao Zhang,[2,4,*] and Naixia Zhang[1,4,6,*]

SUMMARY

Hsp90 is a target for anti-cancer drug development. Both the conformational events tuned by ATP/ADP and co-chaperones and the chaperoning cycle timing are required for Hsp90's fully functional display. Interfering with either one of the conformational events or the cycle timing will down-regulate Hsp90's function. In this manuscript, non-covalent allosteric modulators (SOMCL-16-171 and SOMCL-16-175) targeting Hsp90α's middle domain (Hsp90M) were developed for the first time. Multiple techniques were then applied to characterize the interactions between two active compounds and Hsp90α. Two loops and one α-helix (F349-N360, K443-E451, and D372-G387) in Hsp90M were identified responsible for the recognition of SOMCL-16-171 and SOMCL-16-175. Meanwhile, the binding of SOMCL-16-171 and SOMCL-16-175 to Hsp90M was demonstrated to allosterically modulate the structure and function of Hsp90α's N-terminal domain. Finally, cellular assays were conducted to evaluate the cellular activity of SOMCL-16-175, and the results indicate that SOMCL-16-175 destabilizes Hsp90's client proteins and reduces cell viability.

INTRODUCTION

Protein is the main executor of life activity, and maintenance of proper protein homeostasis is essential for cell viability and growth. Protein degradation pathways (ubiquitin-proteasome system and autophagy-lysosomal pathway) and molecular chaperones, which facilitate protein folding, play central roles in maintaining protein homeostasis of living systems. Hsp90 family is a member of molecular chaperone families. And it is specified by assisting the maturation of hundreds of selected client proteins including transcription factors, steroid hormone receptors, and signaling kinases (Pearl and Prodromou, 2006; Prodromou, 2016, 2017; Schopf et al., 2017). By collaborating to maintain the activity of numerous proteins involved in signaling pathways and cell-cycle control, Hsp90 plays key roles in cellular signal transduction and cell growth.

In eukaryotes, such as *S. cerevisiae* and *Homo sapiens*, two cytosolic isoforms of Hsp90 are encoded and expressed: Hsc82 and Hsp82 in *S. cerevisiae* and Hsp90α and Hsp90β in *Homo sapiens*. Hsc82 and Hsp90β are constitutively expressed, whereas the levels of Hsp82 and Hsp90α are significantly up-regulated under stressful conditions, including heat shock and hypoxia (Zuehlke et al., 2015). For the human paralog Hsp90α, pathological changes including cancer can also stimulate its expression (Zuehlke et al., 2015). Owing to the involvement in cell growth and the up-regulation in multiple types of cancer, Hsp90α is becoming a promising target for anti-cancer drug development (Garg et al., 2016; Prodromou, 2009; Sidera and Patsavoudi, 2014).

Although Hsp90 homologs are expressed in a variety of organisms from bacteria to mammals, they share similar structure and function (Figure S1) (Pearl and Prodromou, 2006; Prodromou, 2016, 2017; Schopf et al., 2017). Hsp90 contains three well-defined structural domains: an N-terminal ATP binding domain (NTD) for ATP-binding and hydrolysis, a middle domain (MD) for client protein recognition, and a C-terminal domain (CTD) mediating Hsp90's dimerization. Hsp90 is tightly regulated by endogenous small molecules such as ATP and ADP by binding to its NTD, and co-chaperone proteins (Hop, Hsp70-Hsp90 organizing protein; p23, 23 kDa protein; Cdc37, protein encoded by the cell division cycle 37 gene; and Aha1, activator of Hsp90 ATPase 1) interacting with the subdomains of the chaperone (Ali et al., 2006; Karagoz et al., 2011; Meyer et al., 2004; Panaretou et al., 2002; Pearl and Prodromou, 2006; Prodromou, 2016, 2017; Schopf et al., 2017; Siligardi et al., 2002, 2004; Vaughan et al., 2008). Hsp90 possesses ATPase activity, and the

[1]Department of Analytical Chemistry, Shanghai Institute of Materia Medica, Chinese Academy of Sciences, 555 Zu Chong Zhi Road, Shanghai 201203, China

[2]CAS Key Laboratory of Receptor Research, Shanghai Institute of Materia Medica, Chinese Academy of Sciences, Shanghai 201203, China

[3]National Facility for Protein Science in Shanghai, ZhangJiang Lab, Shanghai Advanced Research Institute, Chinese Academy of Sciences, Shanghai 201210, China

[4]University of the Chinese Academy of Sciences, 19A Yuquan Road, Beijing 100049, China

[5]These authors contributed equally

[6]Lead Contact

*Correspondence: ycxu@simm.ac.cn (Y.X.), aozhang@simm.ac.cn (A.Z.), nxzhang@simm.ac.cn (N.Z.)

https://doi.org/10.1016/j.isci.2020.100857

binding and hydrolysis of ATP will drive conformational changes of Hsp90 associated with its different function stages: in the apo state, Hsp90 exists in a "V"-shaped conformation dimerized via its CTD; with the binding of ATP, a dimerization of Hsp90's NTD occurs, and co-chaperone proteins and client proteins are recruited; with the hydrolysis of ATP and the releasing of ADP, Hsp90 goes back to the apo "V"-shaped conformation (Pearl and Prodromou, 2000, 2001, 2006; Prodromou, 2012; Prodromou et al., 2000; Prodromou and Pearl, 2003). As mentioned above, tens of co-chaperones are involved in regulating the activity of Hsp90 by interacting with the chaperone protein. For example, the TPR domain (the tetratricopeptide repeat domain) of Hop could interact with the extreme C-terminal MEEVD motif (element containing conserved amino acid sequence of MEEVD) of Hsp90 and the middle domain of Cdc37 could bind to Hsp90 NTD. The binding of either of these two co-chaperones will inhibit Hsp90's ATPase activity and hinder the dimerization of the NTD of the chaperone with the presence of ATP (Roe et al., 2004; Siligardi et al., 2002; Vaughan et al., 2006; Zuehlke and Johnson, 2010). p23 is another well-studied inhibitory co-chaperone of Hsp90. It stabilizes the closed active form of Hsp90 and slows down its ATPase cycle by binding to the dimerized NTD of the chaperone (Ali et al., 2006; Karagoz et al., 2011; Martinez-Yamout et al., 2006; Zuehlke and Johnson, 2010). Among the identified co-chaperones of Hsp90, Aha1 is the only one that was reported to up-regulate the ATPase activity of the chaperone. During the chaperone cycle, Aha1's N-terminal domain binds to Hsp90's MD and induces a consequential conformation change in the MD of Hsp90. After that, the C-terminal domain of Aha1 interacts with Hsp90's NTD and promotes its ATPase activity (Meyer et al., 2004; Panaretou et al., 2002; Prodromou, 2016, 2017; Zuehlke and Johnson, 2010).

As mentioned earlier, the activity of Hsp90 is finely tuned by ATP/ADP and co-chaperones, and an efficient intervention of Hsp90's function could be achieved by interfering with one of the tuning steps in the working cycle of the chaperone. Multiple exogenous small molecules targeting the different structural domains of Hsp90 have been developed. They regulate Hsp90's function mainly via five ways: ATP competitive inhibitors, which block the access of ATP to the Hsp90's NTD (Prodromou, 2009; Roe et al., 1999; Sidera and Patsavoudi, 2014; Verma et al., 2016); inhibitors binding to the Hsp90's NTD and interfering with the interactions between Hsp90 and co-chaperones such as p23 and Cdc37 (Li et al., 2009, 2018; Verma et al., 2016); compounds interacting with Hsp90's CTD and inhibiting its dimerization (Garg et al., 2016; Verma et al., 2016); allosteric activators binding to either the N-terminal domain or the interface region in between the middle domain and the C-terminal domain of Hsp90 (Bassanini et al., 2018; D'Annessa et al., 2017; Ferraro et al., 2019; Sattin et al., 2015; Yokoyama et al., 2015; Zierer et al., 2016; Zierer et al., 2014); and small molecules covalently bonding to the cysteine residue in the middle domain of Hsp90 (Li et al., 2016; Nakamoto et al., 2018; Zhang et al., 2018). Among the reported chemical compounds targeting Hsp90, ATP competitive inhibitors form a dominant group, and quite a few compounds from this group are undergoing clinical trials for the treatment of cancer (Nabi et al., 2018; Sidera and Patsavoudi, 2014; Tatokoro et al., 2015). Unfortunately, up to date, none of these inhibitors has been approved for cancer therapy. This could be at least partially attributed to the pro-survival heat shock response induced by the application of Hsp90 NTD inhibitors, which may compromise their therapeutic potential (Garg et al., 2016). A large number of inhibitors have been developed to target Hsp90 NTD, but only one non-covalent inhibitor (gambogic acid) selectively binding to Hsp90β's middle domain has been reported (Yim et al., 2016). Meanwhile, no known non-covalent modulator targeting the middle domain of Hsp90α, which is the most pronounced target for anti-cancer drug development among Hsp90 paralogs, has been discovered yet. Client protein recognition via protein-protein interaction is the major function of Hsp90α's middle domain (Meyer et al., 2003; Prodromou and Pearl, 2003). No binding pocket for small molecules has been experimentally identified for it. In this manuscript, the fragment-based lead compound discovery approach was applied to explore the possible binding cavity for exogenous modulators in Hsp90α's middle domain. Two active compounds were then obtained. The findings through conducting biophysical and biochemical assays demonstrate that the active compounds could bind to the middle domain of Hsp90α and allosterically modulate the function of the chaperone. More interestingly, these allosteric modulators act as artificial activating co-chaperones of Hsp90α and accelerate its ATPase activity *in vitro*. Finally, cellular assays were subjected to test the *in vivo* activities of obtained allosteric modulators. Anti-proliferation effects and down-regulation of representative Hsp90's clients were observed in breast cancer cell lines upon the application of these compounds.

RESULTS

Structural Characterization of Hsp90α's Middle Domain

The good dispersion of the correlation peaks for amide nitrogen and amide proton atoms in [^{1}H, ^{15}N] HSQC spectrum ([^{1}H, ^{15}N] heteronuclear single quantum correlation spectrum) of Hsp90M indicates

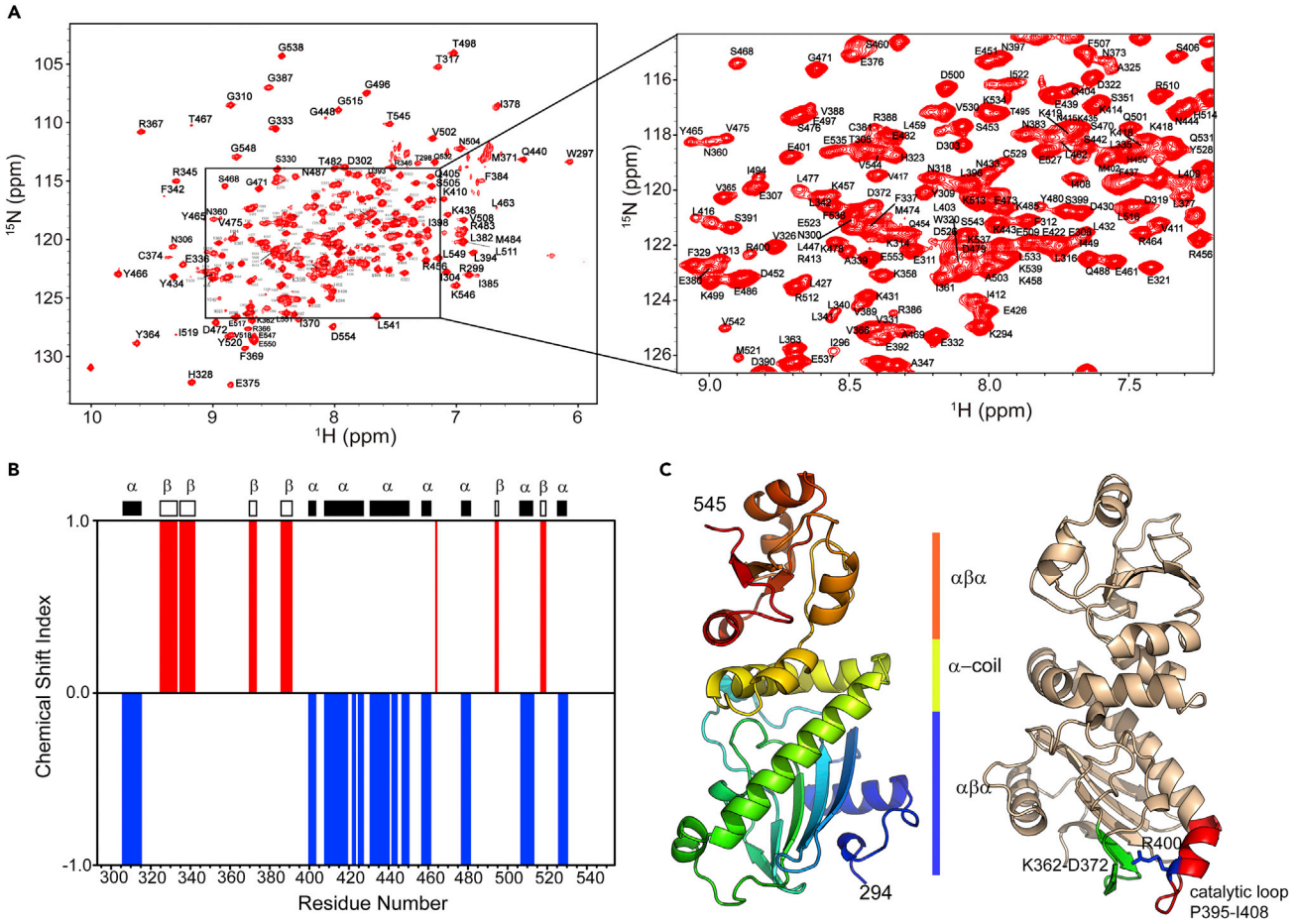

Figure 1. Structural Characterization of Hsp90α's Middle Domain

(A) [^{1}H, ^{15}N] HSQC spectra of the human Hsp90α's middle domain in its free state. Backbone amide resonance assignments are labeled with one-letter amino acid code and sequence number. Regions with cross-peaks partially overlapped are zoomed in.

(B) Chemical shift indices for the C′, Cα, and Cβ atoms of Hsp90α's middle domain reveal its secondary structure. Identified β-strands and α-helices are presented by non-filled rectangles and filled rectangles, respectively. Unassigned residues were excluded from this analysis.

(C) Ribbon representation of the crystal structure of Hsp90α's middle domain (PDB: 6KSQ). The catalytic loop region spanning P395-I408 and its spatially adjacent fragment spanning K362-D372 are highlighted and labeled.

that it is well structured in solution (Figure 1A). The backbone resonance assignments for Hsp90M in its free state have been reported (Park et al., 2011a). These existing assignments are transferred onto our spectra and checked by 3D triple-resonance experiments including HNCA/HNCOCA, HNCO/HNCACO, and HNCACB/CACBCONH. Owing to the large size of Hsp90M, all of the 3D triple-resonance experiments were recorded by using TROSY (transverse relaxation optimized spectroscopy) scheme incorporated pulse sequences and ^{15}N, ^{13}C, and 70% deuterium labeled samples at 0.4 mM. Eventually, the resonances for 228 residues of a total number of 255 non-proline ones were assigned (Figure 1A). It is worth noting that the amide resonances for most of the amino acid residues in two regions including F349-K356 and K489-Y493 were entirely absent from the recorded spectra. The absence of these resonances suggests that they undergo slow conformational exchange in solution (Matsuo et al., 1999). Secondary structural elements of Hsp90M were identified by comparing the chemical shift values of CO, CA, and CB atoms with those of the corresponding residues in randomly coiled structures (Figure 1B). This analysis revealed Hsp90M to be highly structured in solution with eight α-helices and six β-strands spanning its sequence, which indicates that the global fold of Hsp90M in solution state is similar to the folding pattern revealed by its crystal structure (PDB: 6KSQ) (Figure 1C).

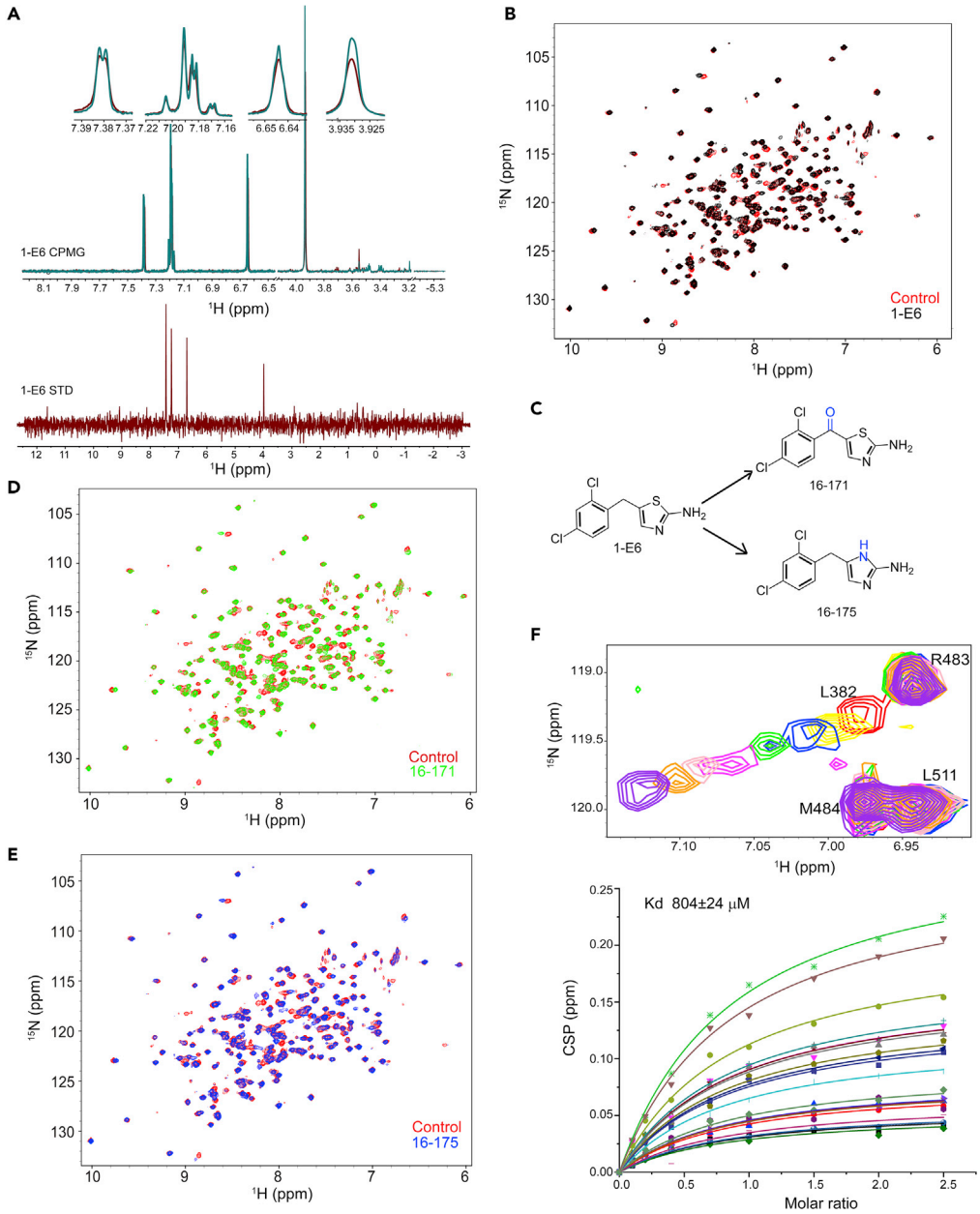

Figure 2. Hit Compound 1-E6 and Its Derivatives SOMCL-16-171 and SOMCL-16-175 Interact with Hsp90α's Middle Domain

(A) Ligand observed CPMG and STD spectra indicate that **1-E6** directly interacts with Hsp90α's middle domain.

(B) The specific interactions between **1-E6** and Hsp90α's middle domain were confirmed by [^{1}H, ^{15}N] HSQC titration experiments. Superposition of [^{1}H, ^{15}N] HSQC spectra of Hsp90α's middle domain without (red) and with **1-E6** (black, molar ratio of 1:4 Hsp90α middle domain to **1-E6**) reveals spectral changes upon hit compound binding.

(C) Chemical structures of **1-E6**, **SOMCL-16-171**, and **SOMCL-16-175**.

(D) The specific interactions between **SOMCL-16-171** and Hsp90α's middle domain were demonstrated by [^{1}H, ^{15}N] HSQC titration experiments. Superposition of [^{1}H, ^{15}N] HSQC spectra of Hsp90α's middle domain without the presence of **SOMCL-16-171** (red) and with the presence of **SOMCL-16-171** (green, molar ratio of 1:4 Hsp90α's middle domain to **SOMCL-16-171**) reveals spectral changes upon compound binding. (E) The specific interactions between **SOMCL-16-175** and Hsp90α's middle domain were demonstrated by [^{1}H, ^{15}N] HSQC titration experiments. Superposition of [^{1}H, ^{15}N] HSQC spectra of Hsp90α's middle domain without the presence of **SOMCL-16-175** (red) and with the presence of **SOMCL-16-175** (blue, molar ratio of 1:4 Hsp90α's middle domain to **SOMCL-16-175**) reveals spectral changes upon compound binding.

Figure 2. *Continued*

(F) Zoomed view of the superposition of [^{1}H, ^{15}N] HSQC spectra of Hsp90α middle domain upon the titration of **SOMCL-16-175**. The spectra are colored according to the molar ratio of Hsp90α middle domain to **SOMCL-16-175** applied in spectrum acquisition: 1:0 (red), 1:1 (yellow), 1:2 (blue), 1:4 (green), 1:7 (magenta), 1:10 (pink), 1:15 (orange), 1:25 (purple). The dissociation constant for the binding of **SOMCL-16-175** to Hsp90α middle domain was determined by the global fitting analysis of CSP data.

Hit Generation and Medicinal Chemistry Optimization

In a previous work, we have setup an NMR-based platform (nuclear magnetic resonance spectroscopy-based platform) for fragment-based lead discovery, which includes a fragment library containing 539 compounds (Yu et al., 2016). Ligand-detected NMR approaches (Carr-Purcell-Meiboom-Gill relaxation dispersion NMR spectroscopy [CPMG], saturation transfer difference NMR spectroscopy [STD], and others) and target-detected NMR methods ([^{1}H, ^{15}N] HSQC and [^{1}H, ^{13}C] HSQC) are two major classes of NMR techniques that are commonly used for the NMR screening of hit compounds (Campos-Olivas, 2011). In this study, ligand-detected NMR approaches including CPMG and STD were applied in the Hsp90α middle domain-targeted hit compound screening toward the fragment library. After the primary group screening and the second cycle of single compound evaluation, one hit compound **1-E6** was identified (Figures 2A and S2). [^{1}H, ^{15}N] HSQC spectra of Hsp90M without or with the presence of **1-E6** confirm that the hit compound could interact with Hsp90M (Figure 2B). Since ATP competitive inhibitors targeting Hsp90's N-terminal domain compose a dominant class of exogenous molecules with the activity of modulating Hsp90's function, [^{1}H, ^{15}N] HSQC titration experiments were done to test if **1-E6** could interact with Hsp90's N-terminal domain. We then found, upon the addition of **1-E6**, that a minor spectral change was observed for Hsp90's N-terminal domain (Figure S3A). These data indicate that **1-E6** has a weak interaction with Hsp90's N-terminal domain. However, the interaction between **1-E6** and Hsp90's N-terminal domain shows no significant effect on **1-E6**'s binding to the middle domain of the chaperone (Figure S3B). There is no significant difference on the **1-E6**-induced spectral changes of Hsp90's middle domain without or with the presence of its N-terminal domain (Figure S3B).

Subsequently, a medicinal chemistry campaign was conducted to optimize the hit compound **1-E6** (Figure S4). First, a global manipulation of **1-E6** was initiated, including replacement of the di-chloro substitution pattern with diverse mono- or multiple halogen or non-halogen substituents, changing the methylene linker with longer alkyl or with heteroatom-containing linkers, as well as substitution of the thiazol-2-amino with alkyl or acyl groups. This round of optimization led to identification of compound **SOMCL-16-171** (Figure 2C), showing more potency and specificity against Hsp90M. Meanwhile, a further focused optimization of the thiazole with various heterocycles yielded compound **SOMCL-16-175** (Figure 2C), which showed even slightly higher potency. The binding of **SOMCL-16-171** and **SOMCL-16-175** to human Hsp90α and yeast Hsp82 (Hsp90α yeast homolog) was confirmed by ligand-detected CPMG and STD NMR data (Figures S5 and S6). Besides, compared with **1-E6**, both **SOMCL-16-171** and **SOMCL-16-175** are more potent Hsp90M modulators with enhanced CSP (chemical shift perturbation) effects upon binding (Figures 2D and 2E). The binding affinity of **SOMCL-16-175** to Hsp90M was determined to be 804 μM (Figure 2F). Meanwhile, the weak binding observed for **1-E6** to Hsp90's N-terminal domain is almost fully (**SOMCL-16-171**) or completely (**SOMCL-16-175**) abolished through compound optimization (Figure S5).

SOMCL-16-171 and SOMCL-16-175 Are Allosteric Modulators of Hsp90α

Hsp90 contains three defined structural domains: an N-terminal ATP binding domain (NTD), a middle domain (MD) for client protein recognition, and a C-terminal domain (CTD) (Figure 3). The ATP binding and hydrolysis in Hsp90's N-terminal domain will trigger sequential conformation changes in both Hsp90's N-terminal domain and its middle domain, and these two domains work cooperatively in the chaperone cycle of Hsp90 (Prodromou, 2012, 2016). Therefore, the binding of **SOMCL-16-171** and **SOMCL-16-175** to Hsp90α's middle domain could potentially show allosteric modulation effects on the N-terminal domain of the chaperone. In this study, thermal shift assay was first applied to evaluate the global modulation effect of **SOMCL-16-171**/**SOMCL-16-175** on Hsp90α. Negative *Tm* shifts for Hsp90NMΔ (human Hsp90α's NTD and MD with the charged linker in between deleted), Hsp90 (human Hsp90α), and Hsp82 (Hsp90α yeast homolog) were observed upon the binding of **SOMCL-16-171** and **SOMCL-16-175** (Figures 3 and S7), which indicate that the binding of the compounds could induce structural changes of Hsp90α and decrease its thermal stability. The thermal shift data suggest that **SOMCL-16-171** and **SOMCL-16-175** could potentially work as allosteric modulators of Hsp90α.

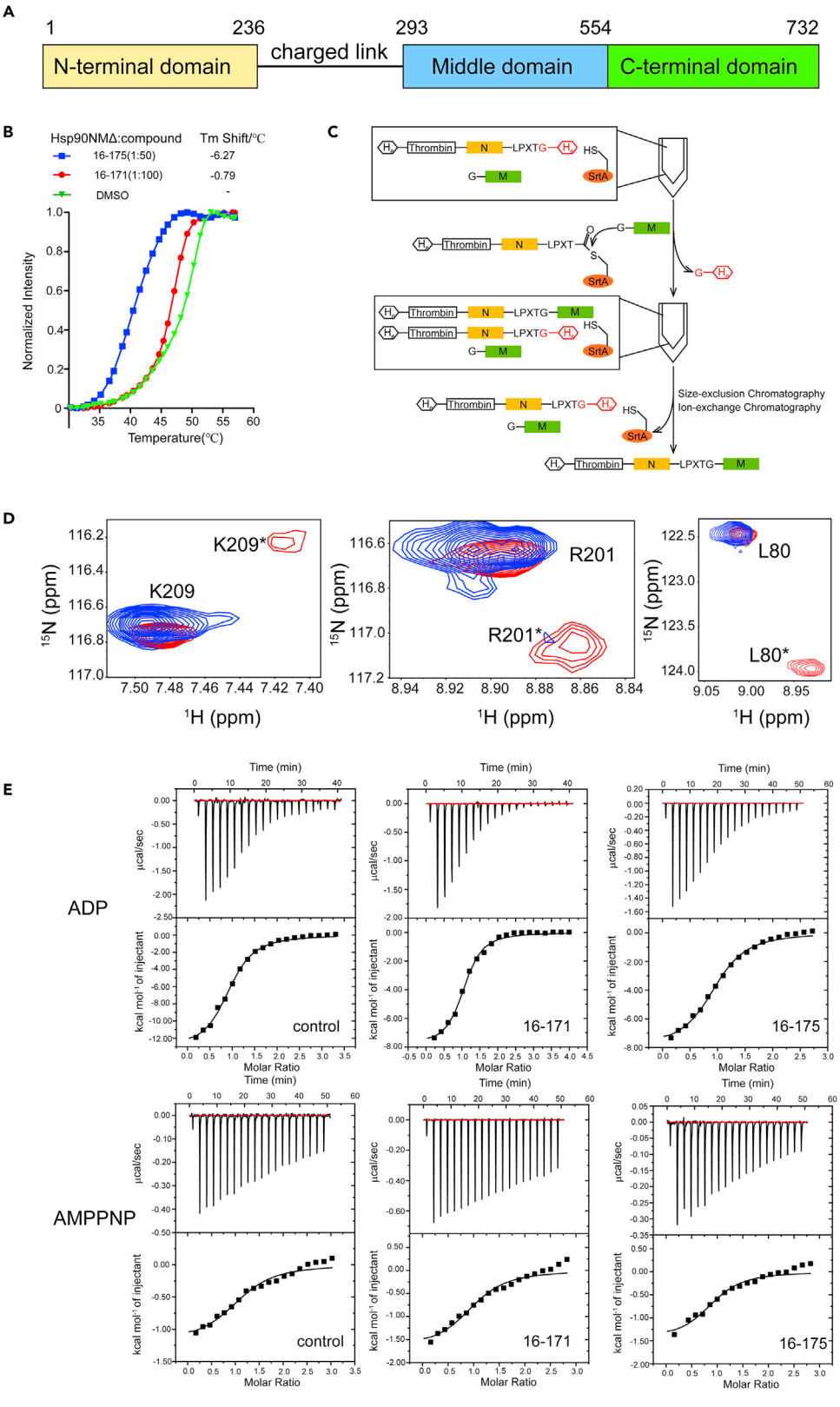
A
1
236
293
554
732
N-terminal domain
charged link
Middle domain
C-terminal domain
B
Hsp90NMΔ:compound
Tm Shift/℃
16-175(1:50)
-6.27
16-171(1:100)
-0.79
DMSO
-
Normalized Intensity
Temperature(℃)
C
Thrombin
N
LPXTG
HS
SrtA
G
M
LPXT
Size-exclusion Chromatography
Ion-exchange Chromatography
D
K209*
K209
R201
R201*
L80
L80*
15N (ppm)
1H (ppm)
E
ADP
AMPPNP
Time (min)
µcal/sec
kcal mol-1 of injectant
Molar Ratio
control
16-171
16-175

Figure 3. SOMCL-16-171 and SOMCL-16-175 Are Allosteric Modulators of Hsp90α

(A) Schematic demonstration of Hsp90's domain architecture.

(B) The shifts in *Tm* values of Hsp90NMΔ (human Hsp90α's NTD and MD with the charged linker in between deleted) upon the binding of **SOMCL-16-171** or **SOMCL-16-175** were determined.

(C) Schematic demonstration of the *in vitro* synthesis of Hsp90NMΔ with its N-terminal domain isotope labeled.

(D) [^{1}H, ^{15}N] HSQC experiments recorded on Hsp90NMΔ with its N-terminal domain ^{15}N labeled without (red) or with the presence of **SOMCL-16-171** (blue) reveal specific residues such as K209, R201, and L80 to undergo conformational shifts when the compound is present. One of the two conformations adopted by the specific residues in Hsp90's N-terminal domain is demoted by the binding of the compound.

(E) Isothermal titration calorimetry experiments were applied to determine the thermodynamic parameters for the binding of ADP (upper panel) or AMPPNP (lower panel) to Hsp90NMΔ premixed with DMSO or either one of two active compounds (**SOMCL-16-171**, **SOMCL-16-175**). The fitting thermodynamic parameters are summarized in Table 1.

After the evaluation of the global modulation effect of two compounds on Hsp90α by thermal shift assay, the NMR method was further used to verify if the compound binding will affect the structure of Hsp90α's N-terminal domain. To gain a clear view of the possible long-range allosteric modulation effect of the compound on Hsp90α's N-terminal domain, a domain-specific isotope labeling approach was applied (Figure 3). Unlabeled Hsp90M and 100% ^{15}N, 90% deuterium-labeled Hsp90N were expressed in *E. coli* and purified by a combination use of nickel affinity chromatography and size-exclusion chromatography. These two protein samples were then ligated together under the catalysis of the engineered Sortase A, and Hsp90NMΔ sample with its N-terminal domain selectively labeled and detected in NMR experiments was then obtained and submitted to [^{1}H, ^{15}N] HSQC spectrum acquisition. According to the NMR data, multiple amino acid residues including L80 and R201 in Hsp90α's N-terminal domain adopt two conformations in solution (the resonance assignments for Hsp90α's N-terminal domain were extracted from the reported literature [Jacobs et al., 2006; Park et al., 2011b; Zhang et al., 2015]), and two corresponding resonance peaks for each residue were observed (Figure 3). However, with the addition of active compound, one of the two resonance peaks for each amino acid residue disappeared in the recorded [^{1}H, ^{15}N] HSQC spectrum, which indicates that the binding of the compound allosterically shapes the structure of Hsp90α's N-terminal domain (Figure 3).

As mentioned earlier, Hsp90's N-terminal domain has ATPase activity and the ATP binding and hydrolysis are intimately coupled to the function cycle of the chaperone. Therefore, to test if the allosteric modulation of **SOMCL-16-171** and **SOMCL-16-175** on Hsp90α's N-terminal domain will affect its function-coupled states, ITC (isothermal titration calorimetry) experiments were carried out. We then found that in comparison with the Hsp90NMΔ in apo state, the pre-incubation of Hsp90NMΔ with **SOMCL-16-171** or **SOMCL-16-175** only presents minor effects on the binding affinities (Kd values) of ADP and ATP analog (AMPPNP) to Hsp90α's N-terminal domain (Figure 3 and Table 1). However, the contributions of entropy (TΔS) and enthalpy (ΔH) to the binding of ADP and AMPPNP to Hsp90α are modified by the presence of the compounds (Figure 3 and Table 1). The ITC data suggest that, with the addition of the compounds, the entropy contribution (TΔS) for ADP and AMPPNP (especially for ADP) binding are significantly enhanced (Table 1). For example, when **SOMCL-16-171** and **SOMCL-16-175** were not or were pre-mixed with Hsp90NMΔ, the TΔS values for ADP:Hsp90NMΔ system were determined to be −4.84, −0.41, and −1.16 kcal·mol^{-1}, respectively (Table 1). The observed gain in entropy for AMPPNP/ADP:Hsp90NMΔ systems could be attributed to the conformational changes of Hsp90NMΔ and/or the perturbation of hydration network of the chaperone protein, which are induced by the binding of **SOMCL-16-171** or **SOMCL-16-175**. Since the water/hydration network could be considered as a component of protein structure, the perturbation of hydration network caused by ligand binding is therefore intimately coupled to protein conformational changes (Biela et al., 2013; Chandler, 2005; Darby et al., 2019). Therefore, the ITC data confirm that the binding of the active compounds to Hsp90α's middle domain does allosterically modulate the conformations of Hsp90α's N-terminal domain in solution.

Characterization of the Interactions between SOMCL-16-171/SOMCL-16-175 and Hsp90α's Middle Domain

To map the interacting sites of **SOMCL-16-171** and **SOMCL-16-175** in Hsp90α's middle domain, [^{1}H, ^{15}N] HSQC NMR titration experiments were performed (Figure 2). The interactions between Hsp90α's middle domain and two compounds are revealed by the CSP analysis data extracted from the [^{1}H, ^{15}N] HSQC spectra (Figures 4A and 4B). The residues with their chemical shifts perturbed and attenuated significantly upon the addition of **SOMCL-16-171** and **SOMCL-16-175** in Hsp90α's middle domain are identified as

Ligand	Compound	N	Kd (μM)	ΔH (10^3 cal mol^{-1})	TΔS (10^3 cal mol^{-1})
ADP	DMSO	0.982 ± 0.06	7.3 ± 1.0	−11.96 ± 0.4	−4.84
	16–171	1.05 ± 0.02	3.4 ± 0.045	−7.99 ± 0.18	−0.41
	16–175	0.967 ± 0.03	6.3 ± 1.2	−8.37 ± 0.32	−1.16
AMPPNP	DMSO	1.04 ± 0.08	14.1 ± 4.6	−2.27 ± 0.24	4.45
	16–171	1.01 ± 0.07	10 ± 3.7	−1.68 ± 0.16	5.24
	16–175	0.92 ± 0.07	8.7 ± 3.4	−1.46 ± 0.16	5.54

Table 1. Thermodynamic Parameters of the Hsp90NMΔ:ADP and Hsp90NMΔ:AMPPNP Systems Measured by ITC Experiments

follows: L340, K358, N360, I361, K362, L363, D372, N373, C374, E375, E376, I378, L382, N383, F384, I385, R386, G387, S442, K443, N444, G448, I449, E451, I525, D526, E527, Y528, C529, V530, Q531, L533, K534, E535 for **SOMCL-16-171** and L340, N360, I361, K362, L363, D372, N373, C374, E375, I378, E380, L382, F384, I385, R386, G387, Y438, K443, G448, I449, E451, Y465, I522, E523, I525, E527, Y528, C529, V530, K534, E535 for **SOMCL-16-175** (Figures 4A and 4B). The perturbed residues in Hsp90α upon the binding of **SOMCL-16-171** and **SOMCL-16-175** both localize to four fragments spanning N360-L363, D372-G387, K443-E451, and I522-E535, which are spatially close to each other (Figure 4C). And this suggests that these four regions modulate the binding of the compounds to Hsp90M. According to the backbone resonance assignments data, the region spanning F349-K356 of Hsp90M undergoes slow conformational exchange in solution and the resonances of the residues in this region are fully absent from the recorded NMR spectra. The slow conformational exchange in this gate-like fragment is expected to favor the recognition of the active compounds by Hsp90α's middle domain. The conclusion achieved by CSP analysis was further confirmed by the mutagenesis study results. Compared with the binding of **SOMCL-16-175** to wild-type Hsp90M, its interactions with Hsp90M F349A and Hsp90M D350A mutants are almost fully abolished, and its interactions with Hsp90M L382A and Hsp90M K443E mutants induce less significant CSPs of the corresponding residues (Figure S8). Meanwhile, the binding of **SOMCL-16-175** to HSP90M Y528A mutant and its interaction with wild-type Hsp90M induce comparable CSPs of the representative residues (Figure S8). The mutagenesis study data suggest that the α-helix spanning I522-E535 might not be involved in the direct binding of **SOMCL-16-175** and the compound binding cavity in Hsp90M is composed of F349-N360, D372-G387, and K443-E451. The observed significant CSPs in the helical region spanning I522-E535 are most possibly from the conformational changes induced by the compound binding. To further define the binding cavity for **SOMCL-16-175** and reveal the possible binding pose of **SOMCL-16-175** in Hsp90M, molecular docking approach was applied. The docking grid was centered on the centroid of eight residues: Phe349, Leu363, Asp372, Gly387, Lys 443, Glu451, Ile522, and Glu535, which were chosen according to the CSP analysis data. The docking model was then obtained, and the binding pocket composed of F349-N360, D372-G387, and K443-E451 for **SOMCL-16-175** in Hsp90M was confirmed (Figure 4D). According to the published literature, the binding pocket for exogenous small molecules in Hsp90α's middle domain identified by us is also found in Hsp90β's middle domain (Yim et al., 2016).

After the identification of the binding sites of two compounds in Hsp90M, we then tested if the compound binding would allosterically modulate the ATPase activity mainly exerting by Hsp90α's N-terminal domain. As it has been reported, two fragments including K362-D372 and P395-I408 in Hsp90M are involved in the promotion of Hsp90's ATPase activity (Meyer et al., 2003; Prodromou, 2016). P395-I408 is named as the catalytic loop, which promotes the ATP hydrolysis process by moving to an open active state and interacting with the γ-phosphate of ATP through the conserved arginine residue in the fragment (R400 for Hsp90α, Figure 1C) (Meyer et al., 2003; Prodromou, 2016), whereas K362-D372 is spatially adjacent to the catalytic loop (Figure 1C) and is found to indirectly modulate the ATP hydrolysis process by its intimate interactions with the catalytic loop in Hsp90's middle domain (Meyer et al., 2003). According to the [^{1}H, ^{15}N] HSQC titration data, the binding of **SOMCL-16-171** and **SOMCL-16-175** to Hsp90M only induce limited CSPs of the residues in the catalytic loop. However, significant CSPs for a few of residues in the region spanning K362-D372 were observed. Therefore, a detectable allosteric modulation effect on the ATPase activity of Hsp90α is expected. *In vitro* ATP hydrolysis assay with or without the presence of **SOMCL-16-175** was then conducted. The ATP hydrolysis process catalyzed by Hsp82

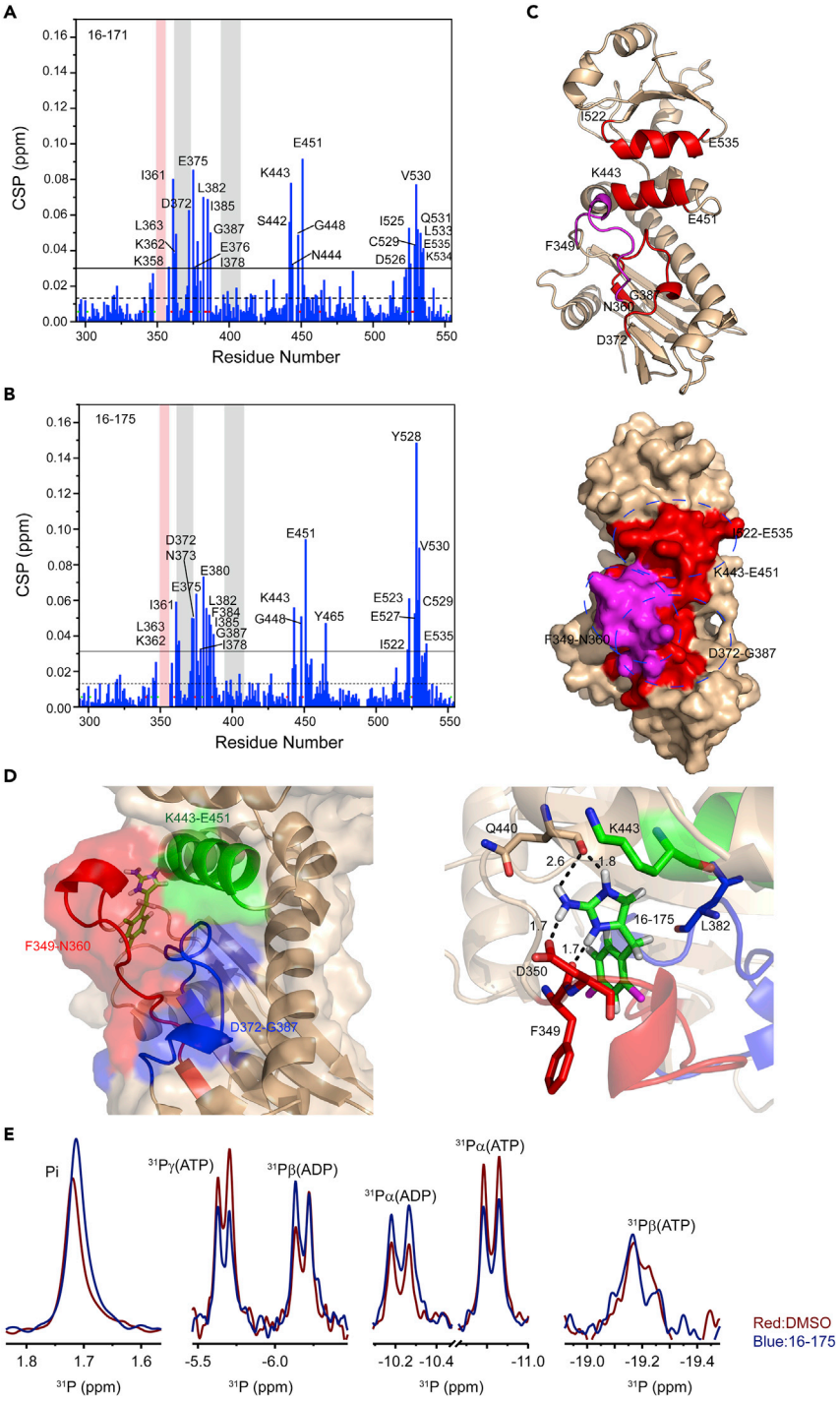

Figure 4. Characterization of the Interactions between SOMCL-16-171/SOMCL-16-175 and Hsp90α's Middle Domain

(A and B) Amide chemical shift perturbation analysis reveals the residues of Hsp90α's middle domain involved in binding SOMCL-16-171 or SOMCL-16-175. The mean and the mean + S.D. value are indicated by dashed line and solid line, respectively. The residues with their CSPs greater than mean + S.D. are labeled. The prolines and the residues with their resonances undergoing significant attenuation upon the addition of SOMCL-16-171 or SOMCL-16-175 are indicated with green dot and red dot, respectively. The catalytic loop (P395-I408) and the β-strands spatially close to it (K362-D372) are highlighted in gray. The fragment spanning F349-K356, which undergoes slow conformational exchange in solution, is highlighted in pink.

Figure 4. *Continued*

(C) According to the CSP data shown in (A) and (B), one loop region spanning D372-G387 and two α-helices including K443-E451 and I522-E535 are identified to play key roles in the recognition of active compounds. These three regions are colored in red in both of the ribbon and the surface presentation of Hsp90M crystal structure (PDB: 6KSQ). The loop region spanning F349-N360, which undergoes conformational exchange in solution and is spatially close to D372-G387 and K443-E451, is colored in magenta.

(D) Expanded view of the possible binding mode of **SOMCL-16-175** to Hsp90α's middle domain. Carbon, nitrogen, chlorine, and hydrogen atoms of the compound are colored green, blue, magenta, and white, respectively. The distances of the hydrogen bonds to **SOMCL-16-175** are provided and indicated in black. Residues L382 and K443, which were selected for mutagenesis study, are highlighted and labeled.

(E) The ^{31}P NMR spectra data suggest that the application of **SOMCL-16-175** promotes the ATPase activity of Hsp82 (Hsp90α yeast homolog). The ATP hydrolysis process catalyzed by Hsp82 was monitored by acquiring 1D ^{31}P spectra. Superposition of 1D ^{31}P spectra of Hsp82:ATP (3 μM:1 mM) reaction system without (red) and with the presence of **SOMCL-16-175** (500 μM, blue) acquired at the time point of 3 h after the initiation of the reaction.

(Hsp90α homolog in yeast) was monitored by acquiring ^{31}P spectra at different time points, and the representative spectra are shown in Figure 4E. At the reaction time point of 3 h after the initiation of the ATP hydrolysis, compared with the reaction system without the presence of **SOMCL-16-175**, higher concentrations of ADP and free phosphate ion and lower concentration of ATP were observed when **SOMCL-16-175** was added (Figures 4 and S9). And these data suggest that the ATPase activity of Hsp90α is promoted by the addition of **SOMCL-16-175**.

SOMCL-16-171 and SOMCL-16-175 Interact with Hsp90 in Cellular Context and Cause Cytotoxicity in Human Breast Cancer Cell Lines

Hsp90 plays important roles in the development of cancers by modulating the maturation of cancer-related client proteins including transcription factors and kinase (Garg et al., 2016; Prodromou, 2009; Sidera and Patsavoudi, 2014). Besides, since Hsp90's chaperone cycle is intimately coupled to the sequential conformation changes induced by endogenous small molecules (ATP and ADP) and co-chaperones (p23, CDC37, Aha1), interfering with any one of the function-related structural states of Hsp90 would present modulation effects on its functional display, which might affect cell growth and proliferation. In this study, cellular thermal shift assay was used to confirm the interaction between **SOMCL-16-171**/**SOMCL-16-175** and Hsp90 in cellular context. In this assay, cell extracts from three breast cancer cell lines, including MDA-MB-231, MCF7, and SKBR3, were pre-incubated with either one of **SOMCL-16-171** and **SOMCL-16-175** or 1% DMSO for 20 min. The mixture samples were then submitted to a parallel incubation lasting for 5 min at different temperatures ranging from 43°C to 67°C. The level of Hsp90 in the after-incubation samples was detected and visualized by using immunoblotting technique (Figures 5A and S12). Compared with the treatment of DMSO, negative shifting of the stability of Hsp90 in the cellular context was observed upon pre-incubation with either **SOMCL-16-171** or **SOMCL-16-175** (Figures 5A, S10, and S12), which suggests that both **SOMCL-16-171** and **SOMCL-16-175** could interact with Hsp90 in the cellular context. After the cellular thermal shift assay, cell viability assay and colony formation experiment were applied to test if the application of **SOMCL-16-171** and **SOMCL-16-175** would cause cytotoxicity. Three breast cancer cell lines, including MDA-MB-231, MCF7, and SKBR3, were used in the experiments. Both the cell viability data and the colony formation results indicate that **SOMCL-16-171** and **SOMCL-16-175** could inhibit cell growth and proliferation (Figures 5 and S10). Moreover, in comparison with **SOMCL-16-171**, the compound **SOMCL-16-175** presents stronger inhibition effects on all of the three cell lines, and the IC50s of **SOMCL-16-175** are 16.48, 34.67, and 13.96 μM for MDA-MB-231, MCF7, and SKBR3, respectively (Figure 5). It is worth noting that the cellular inhibition activity data for **SOMCL-16-171** and **SOMCL-16-175** are consistent with their capacities for down-regulating the thermal stability of Hsp90. With the addition of **SOMCL-16-171** and **SOMCL-16-175**, the *Tm* shifts of Hsp90NMΔ were determined to be −0.79°C and −6.27°C, respectively (Figure 3).

SOMCL-16-175 Promotes the ATPase Activity of Hsp90 and Destabilizes Its Client Proteins

To unravel the potential molecular mechanisms underlying the modulation effects of **SOMCL-16-175** on Hsp90, we analyzed the proteomic changes of MCF7 cells upon the presence of **SOMCL-16-175** by the label-free quantification (LFQ)-based quantitative proteomic method (Figure 6A). Totally, we identified 51,393 peptide sequences, corresponding to 4,866 proteins, with an average of ~30,000 peptide sequences and ~4,500 proteins in each sample (Figures S11A and S11B). The LFQ intensities of identified proteins were

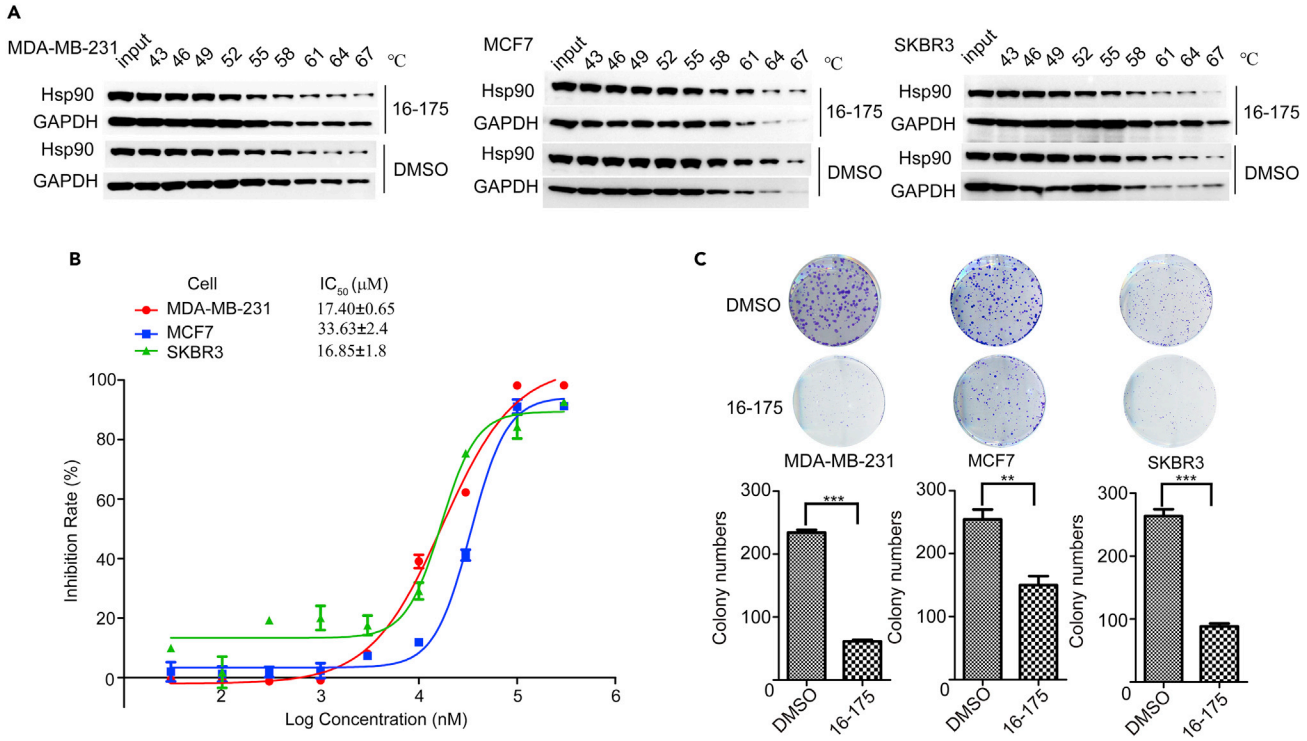

Figure 5. SOMCL-16-175 Interacts with Hsp90 in Cellular Context and Causes Cytotoxicity in Human Breast Cancer Cell Lines

(A) Upon the treatment of **SOMCL-16-175**, decreased thermostability of Hsp90 in cellular context was observed. Extracts from MDA-MB-231, MCF7, and SKBR3 cells were used in the cellular thermal shift experiments.

(B) Cell viability of MDA-MB-231, MCF7, and SKBR3 cells was assessed after exposure to vehicle and different concentrations of **SOMCL-16-175** (30, 100, and 300 nM and 1, 3, 10, 30, 100, and 300 μM) for 72 h. Data are analyzed by GraphPad Prism 5 and presented as means ± S.D. (n = 3).

(C) Colony formation assays were performed on MDA-MB-231, MCF7, and SKBR3 cells treated with different concentrations of **SOMCL-16-175** (7.5 μM for MDA-MB-231 and SKBR3 cells, 17.5 μM for MCF7 cells) for 7–15 days, and quantitative results are shown in lower panel (n = 3, **p < 0.01 compared with control, ***p < 0.0001 compared with control, t test). See also Figure S12.

distributed consistently and correlation coefficients among different samples are 0.97 on average, both demonstrating the high quality of our MS data (Figures S11C and S11D). Principle component analysis (PCA) of the proteomic data indicates a clear separation between the control group and the **SOMCL-16-175**-treated group (Figure 6B). By a global permutation-based FDR approach (Tusher et al., 2001), a total of 458 proteins (up, 180; down, 278) have been revealed to be regulated upon the addition of **SOMCL-16-175** (Figure 6C). Notably, DNA function regulation and cell-cycle-related biological processes are over-represented in the down-regulated proteins (Figure 6D), suggesting the cell cytotoxicity of **SOMCL-16-175**. Quite a few of down-regulated proteins are known clients of Hsp90 and are summarized in Table 2. Among the affected client proteins of Hsp90 (Table 2), the levels of CDK1 (cyclin-dependent kinase 1) and CDK2 (cyclin-dependent kinase 2), which are two of the key players in cell-cycle control, were further tested by using immunoblot approach. Consistent with the proteomic data, significant down-regulation of CDK1 and CDK2 in response to **SOMCL-16-175** treatment was observed (Figures 6E and S12). Meanwhile, CDK4 (cyclin-dependent kinase 4), one of kinase clients of Hsp90, also presents modest decrease in its cellular levels upon the addition of the compound (Figures 6E and S12). Interestingly, although the application of **SOMCL-16-175** destabilizes Hsp90's client proteins (Table 2, Figures 6E and S12), no significant heat-shock response is triggered. Only a minor up-regulation was observed for the level of Hsp70 and Hsp90 upon the treatment of the compound (Figures 6E and S12). Overall, the observed down-regulation of Hsp90's client proteins suggests that the working cycle of the chaperone is finely tuned and the allosteric modulation of the function display of Hsp90 could be achieved by targeting its middle domain.

DISCUSSION

Hsp90 belongs to the chaperone superfamily and plays crucial roles in maintaining the stability and the activity of numerous client proteins, including kinases, transcription factors, and steroid hormone receptors. Owing to its

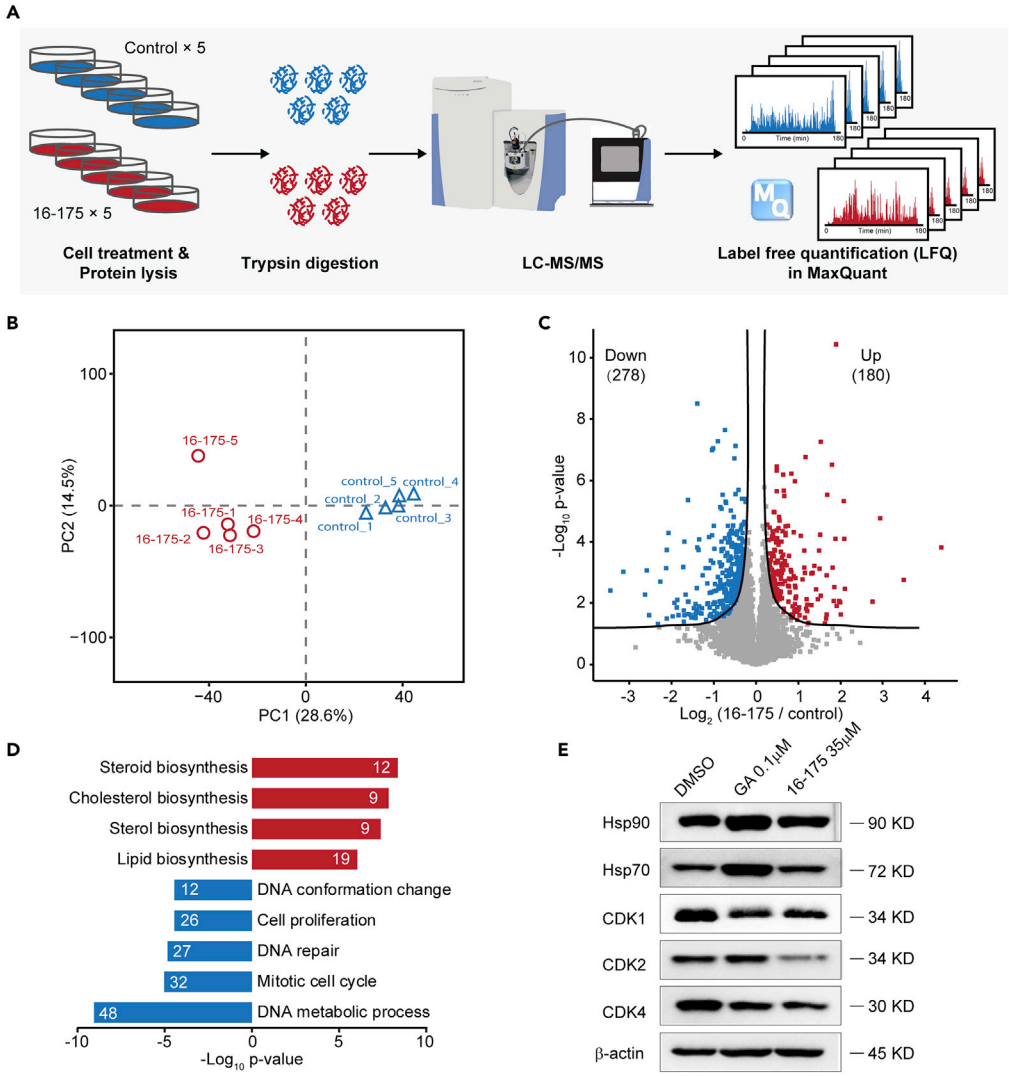

Figure 6. Down-Regulation of the Cell-Cycle Process Revealed by Quantitative Proteomic Analysis

(A) Workflow of the quantitative proteomic analysis. MCF7 cells treated by DMSO control or **SOMCL-16-175** for 48 h were lysed for protein extraction (five replicates for each condition). Peptides were prepared using the FASP (filter-aided sample preparation) method and then subjected to LC-MS/MS analysis using a Q Exactive HF mass spectrometer. Label-free quantification (LFQ) in MaxQuant software was used for relative proteomic quantification.

(B) Principle component analysis (PCA) of the proteomic data for sample replicates. Control and **SOMCL-16-175** samples are clearly separated in PC1, suggesting the differences in proteome between control and **SOMCL-16-175** samples.

(C) Volcano plot reveals the significantly up-regulated and down-regulated proteins in **SOMCL-16-175**-treated samples compared with control, using a global permutation-based FDR approach implemented in Perseus software.

(D) Highly over-represented biological processes in the up-regulated and down-regulated proteins by Fisher's exact test. Protein counts belonging to each process were labeled on the bars.

(E) Consistent with the proteomic analysis results, the immunoblot data also indicate that **SOMCL-16-175** destabilizes Hsp90's client proteins but does not trigger significant heat-shock response. See also Figure S12.

function in controlling the cellular homeostasis of cancer-related proteins such as B-Raf (protein kinase encoded by the BRAF gene), CDK4, and v-src (tyrosine kinase encoded by the v-Src gene), Hsp90 has emerged as a promising target for anti-cancer drug development (Garg et al., 2016; Prodromou, 2009; Sidera and Patsavoudi, 2014). However, although quite a few of candidate compounds targeting the canonical ATP binding pocket in Hsp90's N-terminal domain have stepped into the clinical trial stage, none of them has been approved for cancer therapy. There are multiple reasons that hinder the potential use of Hsp90N-targeted ATP competitive inhibitors in practice. Limited efficacy, pro-survival heat shock response, and poor binding selectivity over Hsp90's different

Uniprot	Protein	References
Q6PJG6	BRAT1 (BRCA1 associated ATM activator 1)	Fierro-Monti et al., 2013
P06493	CDK1 (cyclin-dependent kinase 1)	Garcia-Morales et al., 2007
P24941	CDK2 (cyclin-dependent kinase 2)	Prince et al., 2005
P26358	DNMT1 (DNA (cytosine-5)-methyltransferase 1)	Zhou et al., 2008
Q9Y6Y0	IVNS1ABP (influenza virus NS1A-binding protein)	Zhang et al., 2011
Q99538	LGMN (protein encoded by the LGMN gene)	Lin et al., 2014
Q02750	MAP2K1 (dual specificity mitogen-activated protein kinase kinase 1)	Stancato et al., 1997
P15941	MUC1 (mucin 1)	Ren et al., 2006
Q6P4R8	NFRKB (nuclear factor related to kappa-B-binding protein)	Taipale et al., 2012
P12004	PCNA (proliferating cell nuclear antigen)	Wang et al., 2010
Q96T88	UHRF1 (ubiquitin like with PHD and ring finger domains 1)	Ding et al., 2016

Table 2. Summary of the Down-Regulated Client Proteins of Hsp90 in MCF7 Cells with the Presence of SOMCL-16-175

isoforms compromise their therapeutic potential (Garg et al., 2016; Vartholomaiou et al., 2016). Therefore, developing non-ATP competitive compounds targeting Hsp90 deserves to be tested. In fact, quite a few of research works published during past several years indicate that the allosteric modulators binding to either the N-terminal domain or the interface region in between the middle domain and the C-terminal domain of Hsp90 might serve as new potential therapeutic opportunities (Bassanini et al., 2018; D'Annessa et al., 2017; Ferraro et al., 2019; Sattin et al., 2015; Yokoyama et al., 2015; Zierer et al., 2016; Zierer et al., 2014). Different from the working mode of the canonical ATP competitive inhibitors of Hsp90, the allosteric modulators target the non-canonical binding sites of the chaperone and induce activation of its ATPase activity (D'Annessa et al., 2017; Roe et al., 2018; Sattin et al., 2015; Yokoyama et al., 2015; Zierer et al., 2014). Meanwhile, although presenting accelerating effect on Hsp90's ATP hydrolysis activity, the application of these allosteric modulators would down-regulate the chaperoning function of Hsp90 for client proteins and cause cytotoxicity (D'Annessa et al., 2017; Ferraro et al., 2019; Sattin et al., 2015; Yokoyama et al., 2015; Zierer et al., 2014). These results indicate that the ATPase activity does not fully correlate with the chaperoning activity of Hsp90 (Ferraro et al., 2019). The delicately tuned conformational events and their associated time schedule are both required for the fully functional display of the chaperone. Therefore, both the ATPase inhibitors and the ATPase accelerators would down-regulate Hsp90's cellular activity through perturbing the timing of its chaperoning cycle.

Here in this manuscript, non-covalent allosteric modulators **SOMCL-16-171** and **SOMCL-16-175** targeting Hsp90α's middle domain were discovered by a combination use of experimental screening and medicinal chemistry-guided optimization. Compared with Hsp90α's N-terminal domain, which has a conserved ATP binding pocket shared by GHL-ATPase subfamily members (Dutta and Inouye, 2000), Hsp90α's middle domain mainly functions in client protein recognition (Meyer et al., 2003; Prodromou and Pearl, 2003) and presents no known binding cavity for small molecules. Up to date, only active compounds covalently bonding to the cysteine residue in the middle domain of Hsp90α have been reported. Therefore, fragment-based lead discovery approach, which has been proved to serve as a powerful tool for active compound discovery targeting allosteric binding sites and protein-protein interactions, was applied for Hsp90α's middle domain-targeted hit compound screening. Fortunately, one hit compound **1-E6** from a fragment pool containing 539 compounds was screened out (Figures 2 and S2). After that, medicinal chemistry-guided hit compound optimization was carried out and tens of compounds were synthesized. However, among these compounds, only **SOMCL-16-171** and **SOMCL-16-175** present enhanced CSP effects when binding to Hsp90M (Figure 2). Besides, we found that the optimization attempt through fragment expansion would

decrease the binding capacity of the compound to Hsp90M. It suggests that the volume of the binding pocket in Hsp90M for **1-E6** is quite limited. And this finding is consistent with the aforementioned physiological function of Hsp90α's middle domain. In the following studies, multiple techniques including NMR, ITC, and thermal shift assay were used to confirm and characterize the binding of **SOMCL-16-171** and **SOMCL-16-175** to Hsp90α's middle domain. These two compounds were demonstrated to allosterically modulate the conformation of Hsp90α's N-terminal domain, which consequentially affects the thermodynamics of Hsp90N's interactions with ATP (AMPPNP) and ADP (Figure 3). The CSP analysis data, the mutagenesis study results, and the generated docking model indicate that **SOMCL-16-171** and **SOMCL-16-175** bind to the pocket composed of one α-helix and two loops including K443-E451, F349-N360, and D372-G387 (Figures 4 and S8). And as revealed by the NMR data, loop region F349-K356 undergoes slow conformational exchange in solution, and the resonances for amino acid residues from F349 to K356 are totally absent in the recorded NMR spectra. The high flexibility of F349-K356 is expected to favor the recognition of the active compounds by Hsp90α's middle domain. Meanwhile, as revealed by the CSP analysis data, the binding of **SOMCL-16-175** would induce long-range allosteric modulation effect on the hydrophobic region spanning K362-D372 of Hsp90α's middle domain (Figure 4). Since K362-D372 fragment has been reported to play a role in driving the function-related conformational changes of the catalytic loop in Hsp90's middle domain (Figure 1) (Meyer et al., 2003), we then expect that the binding of **SOMCL-16-171** and **SOMCL-16-175** might modulate the ATPase activity of Hsp90α. This expectation is confirmed by the result of the *in vitro* ATP hydrolysis assay. With the addition of **SOMCL-16-175**, Hsp82 (yeast homolog of Hsp90α) presents an enhancement in its ATPase activity (Figure 4).

As mentioned earlier, the developed allosteric modulators **SOMCL-16-171** and **SOMCL-16-175** could accelerate the ATPase activity of Hsp90 by binding to the pocket composed of F349-N360, K443-E451, and D372-G387 in the middle domain of the chaperone (Figure 4). As it has been known, the co-chaperone Aha1 could stimulate the ATPase activity of Hsp90. The working mode for Aha1:Hsp90 system includes the binding of Aha1's N-terminal domain to Hsp90's middle domain and the nucleotide-dependent binding of Aha1's C-terminal domain to Hsp90's N-terminal domain, which occur in a sequential manner (Retzlaff et al., 2010). A very recent study indicates that the phosphorylation on Y313 of Hsp90's middle domain, which has been reported to promote the recruitment of Aha1 (Xu et al., 2012), would enhance the formation of a transient complex in which both the N-terminal and C-terminal domains of Aha1 bind independently to distinct surfaces of the middle domains in opposing Hsp90 protomers (Xu et al., 2019). Besides, the perturbed residues in the middle domain of Hsp90 Y313E (a phosphomimetic mutation) mutant upon the binding of Aha1 are identified to be I361, I370, I378, I385, I445, I491, I494, and I519 (Xu et al., 2019). Since a few of these residues fall into the **SOMCL-16-171** and **SOMCL-16-175** recognition regions including K443-E451 and D372-G387 in Hsp90's middle domain, binding of the compounds to the chaperone might potentially interfere with the recruitment of Aha1. However, owing to the significant difference in the binding affinities for Aha1 and the developed compound **SOMCL-16-175** to Hsp90, which are 13 (Xu et al., 2012) and 804 μM, respectively, the possible interfering effects are not observable in this study. An allosteric modulator with significantly enhanced binding affinity to the identified pocket in Hsp90's middle domain could serve as a probe molecule to answer the aforementioned question and provide more information for a further understanding of the chaperoning cycle of the chaperone.

After the *in vitro* characterization of the interactions between Hsp90α and the active compounds targeting Hsp90α's middle domain, *in vivo* assays including cell viability assay, colony formation experiment, and mass spectroscopy-based proteomics analysis were carried out to test the cellular activities of the compounds and reveal the underlying molecular mechanisms coupled to their *in vivo* activities. Not surprisingly, both **SOMCL-16-171** and **SOMCL-16-175** cause cytotoxicity in human breast cancer cell lines MDA-MB-231, MCF7, and SKBR3 (Figures 5 and S10). Besides, we found that, among two active compounds, **SOMCL-16-175** shows stronger cytotoxicity than **SOMCL-16-171** (Figures 5 and S10). This is consistent with their *in vitro* characterization data. The binding of **SOMCL-16-175** would induce a much larger *Tm* shift of Hsp90α (Figures 3 and S7). Since **SOMCL-16-175** presents stronger cytotoxicity in breast cancer cell lines, a further proteomics study was applied to investigate the potential working mechanisms linking to the anti-proliferation activity of this compound. Upon the treatment of **SOMCL-16-175**, the down-regulation of the cell-cycle process in MCF7 cell line was revealed by the quantitative proteomic analysis and the decreased levels of multiple key players involved in the cell-cycle pathway were observed (Figure 6). More interestingly, both the proteomic analysis and the immunoblot data demonstrate that no significant heat-shock response is triggered by the treatment of **SOMCL-16-175** (Figures 6 and S12). Although the modest binding of the compound to Hsp90 might potentially contribute to this observation, it is still an

encouraging finding and deserves to be investigated further. To achieve an exclusive conclusion, allosteric modulator with stronger binding affinity to Hsp90α's middle domain needs to be developed and evaluated.

Limitations of the Study

In this study, two allosteric modulators (**SOMCL-16-171** and **SOMCL-16-175**) of Hsp90α were developed. However, these two compounds only present modest binding capabilities to the middle domain of the chaperone. And at least partially due to the low binding affinities, no high-resolution complex structures for Hsp90M:**SOMCL-16-171** and Hsp90M:**SOMCL-16-175** were solved, which would make a further compound optimization derived from **SOMCL-16-171**/**SOMCL-16-175** less efficient.

METHODS

All methods can be found in the accompanying Transparent Methods supplemental file.

DATA AND CODE AVAILABILITY

The accession number for the atomic coordinates of Hsp90M protein reported in this paper is PDB: 6KSQ.

SUPPLEMENTAL INFORMATION

Supplemental Information can be found online at https://doi.org/10.1016/j.isci.2020.100857.

ACKNOWLEDGMENTS

The NMR data were recorded in the Institutional Technological Service Center of Shanghai Institute of Materia Medica and the National Facility for Protein Science in Shanghai of Shanghai Advanced Research Institute. This work was financially supported by the National Natural Science Foundation of China (Grant Nos. 21778061, 81430080, 21977105) and the National Science & Technology Major Project "Key New Drug Creation and Manufacturing Program" of China (Grant No. 2018ZX09711002).

AUTHOR CONTRIBUTIONS

N.Z., A.Z., and Y.X. designed the study; C. Zhou and H.S. solved the crystal structure of Hsp90M; C. Zhou and Z.L. performed the NMR experiments; C. Zhou and N.Z. analyzed the NMR data; A.Z., C. Zhang, and T.C. designed and synthesized the compounds; C. Zhou and X.Z. performed the ITC experiments; Y.X. and M.X. designed and performed the molecular docking; H. Zhu, H. Zhou, and C. Zhou designed and performed the proteomic analysis; C. Zhou performed the cellular assays; C. Zhou, H.H., and Y.Z. prepared the protein samples; N.Z., A.Z., Y.X., C. Zhou, and H. Zhu wrote the manuscript.

DECLARATION OF INTERESTS

The authors declare no competing interests.

Received: September 17, 2019
Revised: December 20, 2019
Accepted: January 15, 2020
Published: February 21, 2020

REFERENCES

Ali, M.M., Roe, S.M., Vaughan, C.K., Meyer, P., Panaretou, B., Piper, P.W., Prodromou, C., and Pearl, L.H. (2006). Crystal structure of an Hsp90-nucleotide-p23/Sba1 closed chaperone complex. Nature *440*, 1013–1017.

Bassanini, I., D'Annessa, I., Costa, M., Monti, D., Colombo, G., and Riva, S. (2018). Chemoenzymatic synthesis of (E)-2,3-diaryl-5-styryl-trans-2,3-dihydrobenzofuran-based scaffolds and their in vitro and in silico evaluation as a novel sub-family of potential allosteric modulators of the 90 kDa heat shock protein (Hsp90). Org. Biomol. Chem. *16*, 3741–3753.

Biela, A., Nasief, N.N., Betz, M., Heine, A., Hangauer, D., and Klebe, G. (2013). Dissecting the hydrophobic effect on the molecular level: the role of water, enthalpy, and entropy in ligand binding to thermolysin. Angew. Chem. Int. Ed. *52*, 1822–1828.

Campos-Olivas, R. (2011). NMR screening and hit validation in fragment based drug discovery. Curr. Top. Med. Chem. *11*, 43–67.

Chandler, D. (2005). Interfaces and the driving force of hydrophobic assembly. Nature *437*, 640–647.

D'Annessa, I., Sattin, S., Tao, J., Pennati, M., Sanchez-Martin, C., Moroni, E., Rasola, A., Zaffaroni, N., Agard, D.A., Bernardi, A., et al. (2017). Design of allosteric stimulators of the Hsp90 ATPase as new anticancer leads. Chemistry *23*, 5188–5192.

Darby, J.F., Hopkins, A.P., Shimizu, S., Roberts, S.M., Brannigan, J.A., Turkenburg, J.P., Thomas, G.H., Hubbard, R.E., and Fischer, M. (2019). Water networks can determine the affinity of ligand binding to proteins. J. Am. Chem. Soc. *141*, 15818–15826.

Ding, G.J., Chen, P.L., Zhang, H., Huang, X.J., Zang, Y., Li, J.W., Li, J., and Wong, J.M. (2016). Regulation of ubiquitin-like with plant homeodomain and RING finger domain 1 (UHRF1) protein stability by heat shock protein 90 chaperone machinery. J. Biol. Chem. *291*, 20125–20135.

Dutta, R., and Inouye, M. (2000). GHKL, an emergent ATPase/kinase superfamily. Trends Biochem. Sci. *25*, 24–28.

Ferraro, M., D'Annessa, I., Moroni, E., Morra, G., Paladino, A., Rinaldi, S., Compostella, F., and Colombo, G. (2019). Allosteric modulators of HSP90 and HSP70: dynamics meets function through structure-based drug design. J. Med. Chem. *62*, 60–87.

Fierro-Monti, I., Echeverria, P., Racle, J., Hernandez, C., Picard, D., and Quadroni, M. (2013). Dynamic impacts of the inhibition of the molecular chaperone Hsp90 on the T-cell proteome have implications for anti-cancer therapy. PLoS One *8*, e80425.

Garcia-Morales, P., Carrasco-Garcia, E., Ruiz-Rico, P., Martinez-Mira, R., Menendez-Gutierrez, M.P., Ferragut, J.A., Saceda, M., and Martinez-Lacaci, I. (2007). Inhibition of Hsp90 function by ansamycins causes downregulation of cdc2 and cdc25c and G(2)/M arrest in glioblastoma cell lines. Oncogene *26*, 7185–7193.

Garg, G., Khandelwal, A., and Blagg, B.S. (2016). Anticancer inhibitors of Hsp90 function: beyond the usual suspects. Adv. Cancer Res. *129*, 51–88.

Jacobs, D.M., Langer, T., Elshorst, B., Saxena, K., Fiebig, K.M., Vogtherr, M., and Schwalbe, H. (2006). NMR backbone assignment of the N-terminal domain of human HSP90. J. Biomol. NMR *36*, 52.

Karagoz, G.E., Duarte, A.M., Ippel, H., Uetrecht, C., Sinnige, T., van Rosmalen, M., Hausmann, J., Heck, A.J., Boelens, R., and Rudiger, S.G. (2011). N-terminal domain of human Hsp90 triggers binding to the cochaperone p23. Proc. Natl. Acad. Sci. U S A *108*, 580–585.

Li, Y., Zhang, T., Jiang, Y., Lee, H.F., Schwartz, S.J., and Sun, D. (2009). (-)-Epigallocatechin-3-gallate inhibits Hsp90 function by impairing Hsp90 association with cochaperones in pancreatic cancer cell line Mia Paca-2. Mol. Pharm. *6*, 1152–1159.

Li, D., Li, C., Li, L., Chen, S., Wang, L., Li, Q., Wang, X., Lei, X., and Shen, Z. (2016). Natural product Kongensin A is a non-canonical HSP90 inhibitor that blocks RIP3-dependent necroptosis. Cell Chem. Biol. *23*, 257–266.

Li, T., Jiang, H.L., Tong, Y.G., and Lu, J.J. (2018). Targeting the Hsp90-Cdc37-client protein interaction to disrupt Hsp90 chaperone machinery. J. Hematol. Oncol. *11*, 59.

Lin, Y.Y., Qiu, Y.M., Xu, C., Liu, Q.L., Peng, B.W., Kaufmann, G.F., Chen, X., Lan, B., Wei, C.Y., Lu, D.S., et al. (2014). Functional role of asparaginyl endopeptidase ubiquitination by TRAF6 in tumor invasion and metastasis. J. Natl. Cancer Inst. *106*, dju012.

Martinez-Yamout, M.A., Venkitakrishnan, R.P., Preece, N.E., Kroon, G., Wright, P.E., and Dyson, H.J. (2006). Localization of sites of interaction between p23 and Hsp90 in solution. J. Biol. Chem. *281*, 14457–14464.

Matsuo, H., Walters, K.J., Teruya, K., Tanaka, T., Gassner, G.T., Lippard, S.J., Kyogoku, Y., and Wagner, G. (1999). Identification by NMR spectroscopy of residues at contact surfaces in large, slowly exchanging macromolecular complexes. J. Am. Chem. Soc. *121*, 9903–9904.

Meyer, P., Prodromou, C., Hu, B., Vaughan, C., Roe, S.M., Panaretou, B., Piper, P.W., and Pearl, L.H. (2003). Structural and functional analysis of the middle segment of Hsp90: implications for ATP hydrolysis and client protein and cochaperone interactions. Mol. Cell *11*, 647–658.

Meyer, P., Prodromou, C., Liao, C., Hu, B., Mark Roe, S., Vaughan, C.K., Vlasic, I., Panaretou, B., Piper, P.W., and Pearl, L.H. (2004). Structural basis for recruitment of the ATPase activator Aha1 to the Hsp90 chaperone machinery. EMBO J. *23*, 511–519.

Nabi, F., Iqbal, M.K., Zhang, H., Rehman, M.U., Shahzad, M., Huang, S., Han, Z., Mehmood, K., Ahmed, N., Chachar, B., et al. (2018). Clinical efficiency and safety of Hsp90 inhibitor Novobiocin in avian tibial dyschondroplasia. J. Vet. Pharmacol. Ther. *41*, 902–911.

Nakamoto, H., Amaya, Y., Komatsu, T., Suzuki, T., Dohmae, N., Nakamura, Y., Jantan, I., and Miyata, Y. (2018). Stimulation of the ATPase activity of Hsp90 by zerumbone modification of its cysteine residues destabilizes its clients and causes cytotoxicity. Biochem. J. *475*, 2559–2576.

Panaretou, B., Siligardi, G., Meyer, P., Maloney, A., Sullivan, J.K., Singh, S., Millson, S.H., Clarke, P.A., Naaby-Hansen, S., Stein, R., et al. (2002). Activation of the ATPase activity of hsp90 by the stress-regulated cochaperone aha1. Mol. Cell *10*, 1307–1318.

Park, S.J., Borin, B.N., Martinez-Yamout, M.A., and Dyson, H.J. (2011a). The client protein p53 adopts a molten globule-like state in the presence of Hsp90. Nat. Struct. Mol. Biol. *18*, 537–541.

Park, S.J., Kostic, M., and Dyson, H.J. (2011b). Dynamic interaction of Hsp90 with its client protein p53. J. Mol. Biol. *411*, 158–173.

Pearl, L.H., and Prodromou, C. (2000). Structure and in vivo function of Hsp90. Curr. Opin. Struct. Biol. *10*, 46–51.

Pearl, L.H., and Prodromou, C. (2001). Structure, function, and mechanism of the Hsp90 molecular chaperone. Adv. Protein Chem. *59*, 157–186.

Pearl, L.H., and Prodromou, C. (2006). Structure and mechanism of the Hsp90 molecular chaperone machinery. Annu. Rev. Biochem. *75*, 271–294.

Prince, T., Sun, L., and Matts, R.L. (2005). Cdk2: a genuine protein kinase client of Hsp90 and Cdc37. Biochemistry *44*, 15287–15295.

Prodromou, C., and Pearl, L.H. (2003). Structure and functional relationships of Hsp90. Curr. Cancer Drug Targets *3*, 301–323.

Prodromou, C. (2009). Strategies for stalling malignancy: targeting cancer's addiction to Hsp90. Curr. Top. Med. Chem. *9*, 1352–1368.

Prodromou, C. (2012). The 'active life' of Hsp90 complexes. Biochim. Biophys. Acta *1823*, 614–623.

Prodromou, C. (2016). Mechanisms of Hsp90 regulation. Biochem. J. *473*, 2439–2452.

Prodromou, C. (2017). Regulatory mechanisms of Hsp90. Biochem. Mol. Biol. J. *3*, 2.

Prodromou, C., Panaretou, B., Chohan, S., Siligardi, G., O'Brien, R., Ladbury, J.E., Roe, S.M., Piper, P.W., and Pearl, L.H. (2000). The ATPase cycle of Hsp90 drives a molecular 'clamp' via transient dimerization of the N-terminal domains. EMBO J. *19*, 4383–4392.

Ren, J., Bharti, A., Raina, D., Chen, W., Ahmad, R., and Kufe, D. (2006). MUC1 oncoprotein is targeted to mitochondria by heregulin-induced activation of c-Src and the molecular chaperone HSP90. Oncogene *25*, 20–31.

Retzlaff, M., Hagn, F., Mitschke, L., Hessling, M., Gugel, F., Kessler, H., Richter, K., and Buchner, J. (2010). Asymmetric activation of the hsp90 dimer by its cochaperone aha1. Mol. Cell *37*, 344–354.

Roe, S.M., Prodromou, C., O'Brien, R., Ladbury, J.E., Piper, P.W., and Pearl, L.H. (1999). Structural basis for inhibition of the Hsp90 molecular chaperone by the antitumor antibiotics radicicol and geldanamycin. J. Med. Chem. *42*, 260–266.

Roe, S.M., Ali, M.M., Meyer, P., Vaughan, C.K., Panaretou, B., Piper, P.W., Prodromou, C., and Pearl, L.H. (2004). The Mechanism of Hsp90 regulation by the protein kinase-specific cochaperone p50(cdc37). Cell *116*, 87–98.

Roe, M.S., Wahab, B., Torok, Z., Horvath, I., Vigh, L., and Prodromou, C. (2018). Dihydropyridines allosterically modulate Hsp90 providing a novel mechanism for heat shock protein Co-induction and neuroprotection. Front. Mol. Biosci. *5*, 51.

Sattin, S., Tao, J., Vettoretti, G., Moroni, E., Pennati, M., Lopergolo, A., Morelli, L., Bugatti, A., Zuehlke, A., Moses, M., et al. (2015). Activation of Hsp90 enzymatic activity and conformational dynamics through rationally designed allosteric ligands. Chemistry *21*, 13598–13608.

Schopf, F.H., Biebl, M.M., and Buchner, J. (2017). The HSP90 chaperone machinery. Nat. Rev. Mol. Cell Biol. *18*, 345–360.

Sidera, K., and Patsavoudi, E. (2014). HSP90 inhibitors: current development and potential in cancer therapy. Recent Pat. Anticancer Drug Discov. *9*, 1–20.

Siligardi, G., Panaretou, B., Meyer, P., Singh, S., Woolfson, D.N., Piper, P.W., Pearl, L.H., and Prodromou, C. (2002). Regulation of Hsp90 ATPase activity by the co-chaperone Cdc37p/p50cdc37. J. Biol. Chem. *277*, 20151–20159.

Siligardi, G., Hu, B., Panaretou, B., Piper, P.W., Pearl, L.H., and Prodromou, C. (2004). Co-chaperone regulation of conformational switching in the Hsp90 ATPase cycle. J. Biol. Chem. *279*, 51989–51998.

Stancato, L.F., Silverstein, A.M., OwensGrillo, J.K., Chow, Y.H., Jove, R., and Pratt, W.B. (1997). The hsp90-binding antibiotic geldanamycin decreases Raf levels and epidermal growth factor signaling without disrupting formation of

signaling complexes or reducing the specific enzymatic activity of raf kinase. J. Biol. Chem. *272*, 4013–4020.

Taipale, M., Krykbaeva, I., Koeva, M., Kayatekin, C., Westover, K.D., Karras, G.I., and Lindquist, S. (2012). Quantitative analysis of Hsp90-client interactions reveals principles of substrate recognition. Cell *150*, 987–1001.

Tatokoro, M., Koga, F., Yoshida, S., and Kihara, K. (2015). Heat shock protein 90 targeting therapy: state of the art and future perspective. EXCLI J. *14*, 48–58.

Tusher, V.G., Tibshirani, R., and Chu, G. (2001). Significance analysis of microarrays applied to the ionizing radiation response. Proc. Natl. Acad. Sci. U S A *98*, 5116–5121.

Vartholomaiou, E., Echeverria, P.C., and Picard, D. (2016). Unusual suspects in the twilight zone between the Hsp90 interactome and carcinogenesis. Adv. Cancer Res. *129*, 1–30.

Vaughan, C.K., Gohlke, U., Sobott, F., Good, V.M., Ali, M.M., Prodromou, C., Robinson, C.V., Saibil, H.R., and Pearl, L.H. (2006). Structure of an Hsp90-Cdc37-Cdk4 complex. Mol. Cell *23*, 697–707.

Vaughan, C.K., Mollapour, M., Smith, J.R., Truman, A., Hu, B., Good, V.M., Panaretou, B., Neckers, L., Clarke, P.A., Workman, P., et al. (2008). Hsp90-dependent activation of protein kinases is regulated by chaperone-targeted dephosphorylation of Cdc37. Mol. Cell *31*, 886–895.

Verma, S., Goyal, S., Jamal, S., Singh, A., and Grover, A. (2016). Hsp90: friends, clients and natural foes. Biochimie *127*, 227–240.

Wang, X., Heuvelman, D.M., Carroll, J.A., Dufield, D.R., and Masferrer, J.L. (2010). Geldanamycin-induced PCNA degradation in isolated Hsp90 complex from cancer cells. Cancer Invest. *28*, 635–641.

Xu, W., Mollapour, M., Prodromou, C., Wang, S., Scroggins, B.T., Palchick, Z., Beebe, K., Siderius, M., Lee, M.J., Couvillon, A., et al. (2012). Dynamic tyrosine phosphorylation modulates cycling of the HSP90-P50(CDC37)-AHA1 chaperone machine. Mol. Cell *47*, 434–443.

Xu, W., Beebe, K., Chavez, J.D., Boysen, M., Lu, Y., Zuehlke, A.D., Keramisanou, D., Trepel, J.B., Prodromou, C., Mayer, M.P., et al. (2019). Hsp90 middle domain phosphorylation initiates a complex conformational program to recruit the ATPase-stimulating cochaperone Aha1. Nat. Commun. *10*, 2574.

Yim, K.H., Prince, T.L., Qu, S.W., Bai, F., Jennings, P.A., Onuchic, J.N., Theodorakis, E.A., and Neckers, L. (2016). Gambogic acid identifies an isoform-specific druggable pocket in the middle domain of Hsp90 beta. Proc. Natl. Acad. Sci. U S A *113*, E4801–E4809.

Yokoyama, Y., Ohtaki, A., Jantan, I., Yohda, M., and Nakamoto, H. (2015). Goniothalamin enhances the ATPase activity of the molecular chaperone Hsp90 but inhibits its chaperone activity. J. Biochem. *157*, 161–168.

Yu, J.L., Chen, T.T., Zhou, C., Lian, F.L., Tang, X.L., Wen, Y., Shen, J.K., Xu, Y.C., Xiong, B., and Zhang, N.X. (2016). NMR-based platform for fragment-based lead discovery used in screening BRD4-targeted compounds. Acta. Pharmacol. Sin. *37*, 984–993.

Zhang, C.F., Yang, Y.T., Zhou, X.W., Yang, Z.X., Liu, X.L., Cao, Z.L., Song, H.B., He, Y.X., and Huang, P.T. (2011). The NS1 protein of influenza a virus interacts with heat shock protein Hsp90 in human alveolar basal epithelial cells: implication for virus-induced apoptosis. Virol. J. *8*, 181.

Zhang, H.Q., Zhou, C., Chen, W.Y., Xu, Y.C., Shi, Y.H., Wen, Y., and Zhang, N.X. (2015). A dynamic view of ATP-coupled functioning cycle of Hsp90 N-terminal domain. Sci. Rep. *5*, 9542.

Zhang, F.Z., Ho, D.H., and Wong, R.H. (2018). Triptolide, a HSP90 middle domain inhibitor, induces apoptosis in triple manner. Oncotarget *9*, 22301–22315.

Zhou, Q., Agoston, A.T., Atadja, P., Nelson, W.G., and Davidson, N.E. (2008). Inhibition of histone deacetylases promotes ubiquitin-dependent proteasomal degradation of DNA methyltransferase 1 in human breast cancer cells. Mol. Cancer Res. *6*, 873–883.

Zierer, B.K., Weiwad, M., Rubbelke, M., Freiburger, L., Fischer, G., Lorenz, O.R., Sattler, M., Richter, K., and Buchner, J. (2014). Artificial accelerators of the molecular chaperone Hsp90 facilitate rate-limiting conformational transitions. Angew. Chem. *53*, 12257–12262.

Zierer, B.K., Rubbelke, M., Tippel, F., Madl, T., Schopf, F.H., Rutz, D.A., Richter, K., Sattler, M., and Buchner, J. (2016). Importance of cycle timing for the function of the molecular chaperone Hsp90. Nat. Struct. Mol. Biol. *23*, 1020–1028.

Zuehlke, A., and Johnson, J.L. (2010). Hsp90 and co-chaperones twist the functions of diverse client proteins. Biopolymers *93*, 211–217.

Zuehlke, A.D., Beebe, K., Neckers, L., and Prince, T. (2015). Regulation and function of the human HSP90AA1 gene. Gene *570*, 8–16.

iScience, Volume *23*

Supplemental Information

Allosteric Regulation of Hsp90α's Activity by Small Molecules Targeting the Middle Domain of the Chaperone

Chen Zhou, Chi Zhang, Hongwen Zhu, Zhijun Liu, Haixia Su, Xianglei Zhang, Tingting Chen, Yan Zhong, Huifang Hu, Muya Xiong, Hu Zhou, Yechun Xu, Ao Zhang, and Naixia Zhang

Supplemental Figures

Figure S1

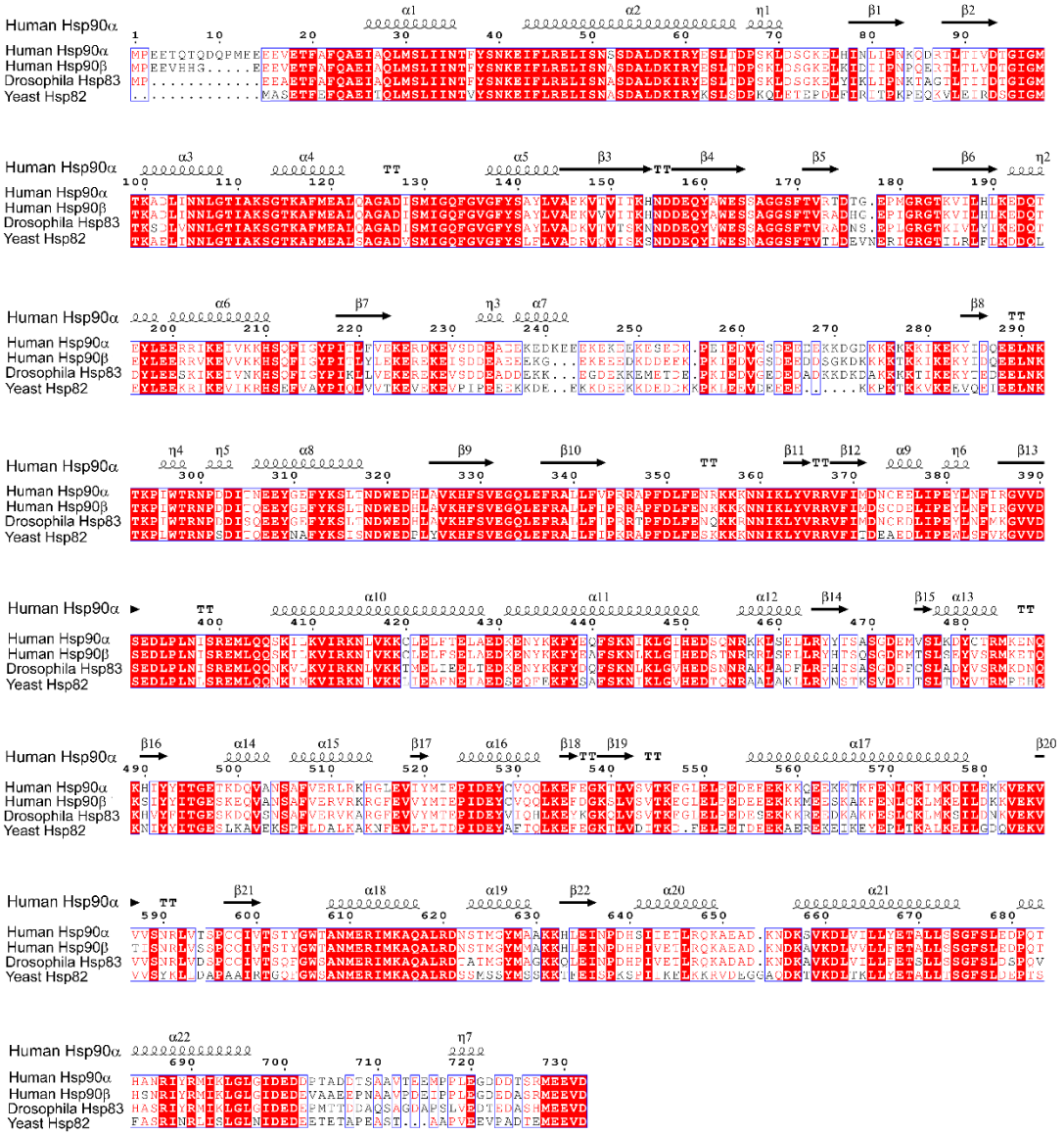

Figure S1. Sequence alignment of representative cytosolic Hsp90 homologs from different species. Related to Figure 1. Conserved residues are marked in red.

Figure S2

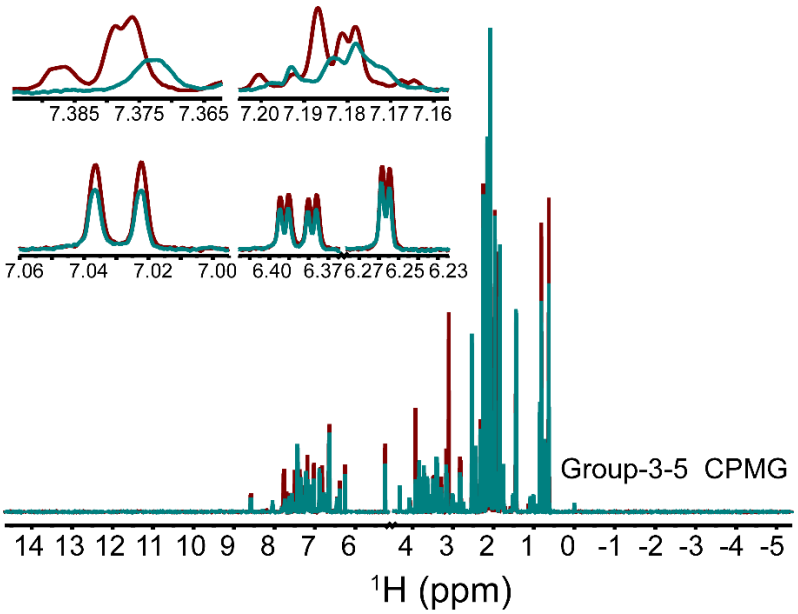

Figure S2. Ligand observed CPMG spectra indicate that 1-E6 in Group-3-5 compound mixture potentially interacts with Hsp90α's middle domain. Related to Figure 2. CPMG NMR spectra for Group-3-5 compound mixture only (200 μM) and Group-3-5 compound mixture (200 μM) with the presence of Hsp90α middle domain (5 μM) are colored in red and cyan, respectively.

Figure S3

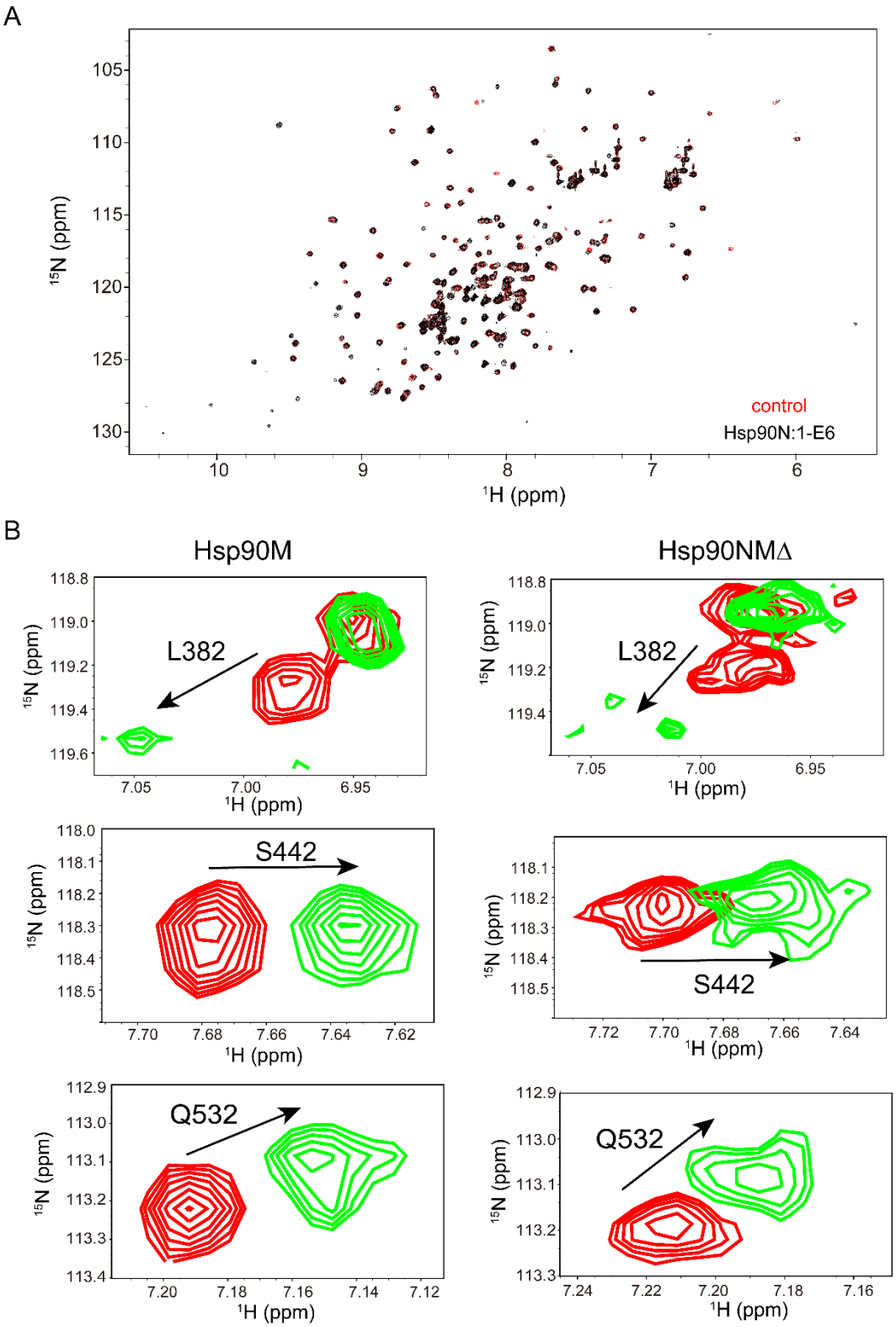

Figure S3. Hit compound 1-E6 has a weak interaction with Hsp90α's N-terminal domain. Related to Figure 2. (A) Superposition of [^{1}H, ^{15}N] HSQC spectra of Hsp90α's N-terminal domain without (red) and with **1-E6** (black, molar ratio of 1:4 Hsp90α N-terminal domain to **1-**

E6) reveals a minor spectral change upon the addition of the compound. (B) The specific interactions between **1-E6** and Hsp90α's middle domain were confirmed by [^{1}H, ^{15}N] HSQC titration experiments. [^{1}H, ^{15}N] HSQC experiments recorded on Hsp90α's middle domain and Hsp90NMΔ with its middle domain ^{15}N labelled without (red) or with the presence of **1-E6** (green) reveal significant spectral changes when the compound is present.

Figure S4

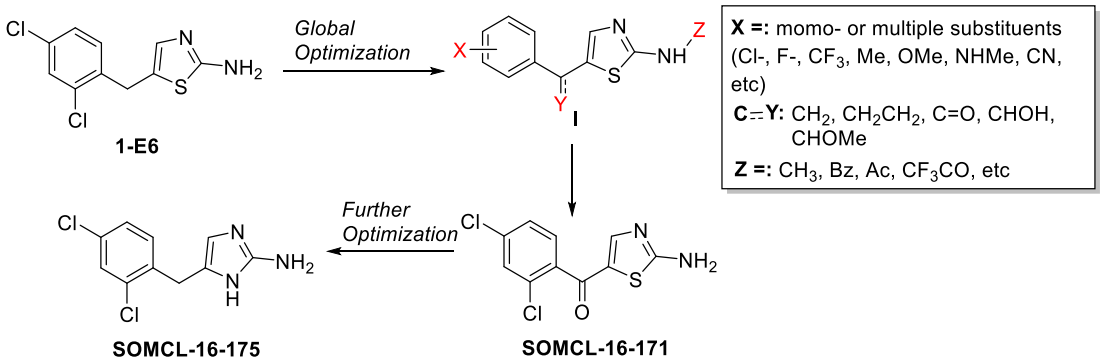

Figure S4. Medicinal chemistry optimization of the hit compound 1-E6. Related to Figure 2.

Figure S5

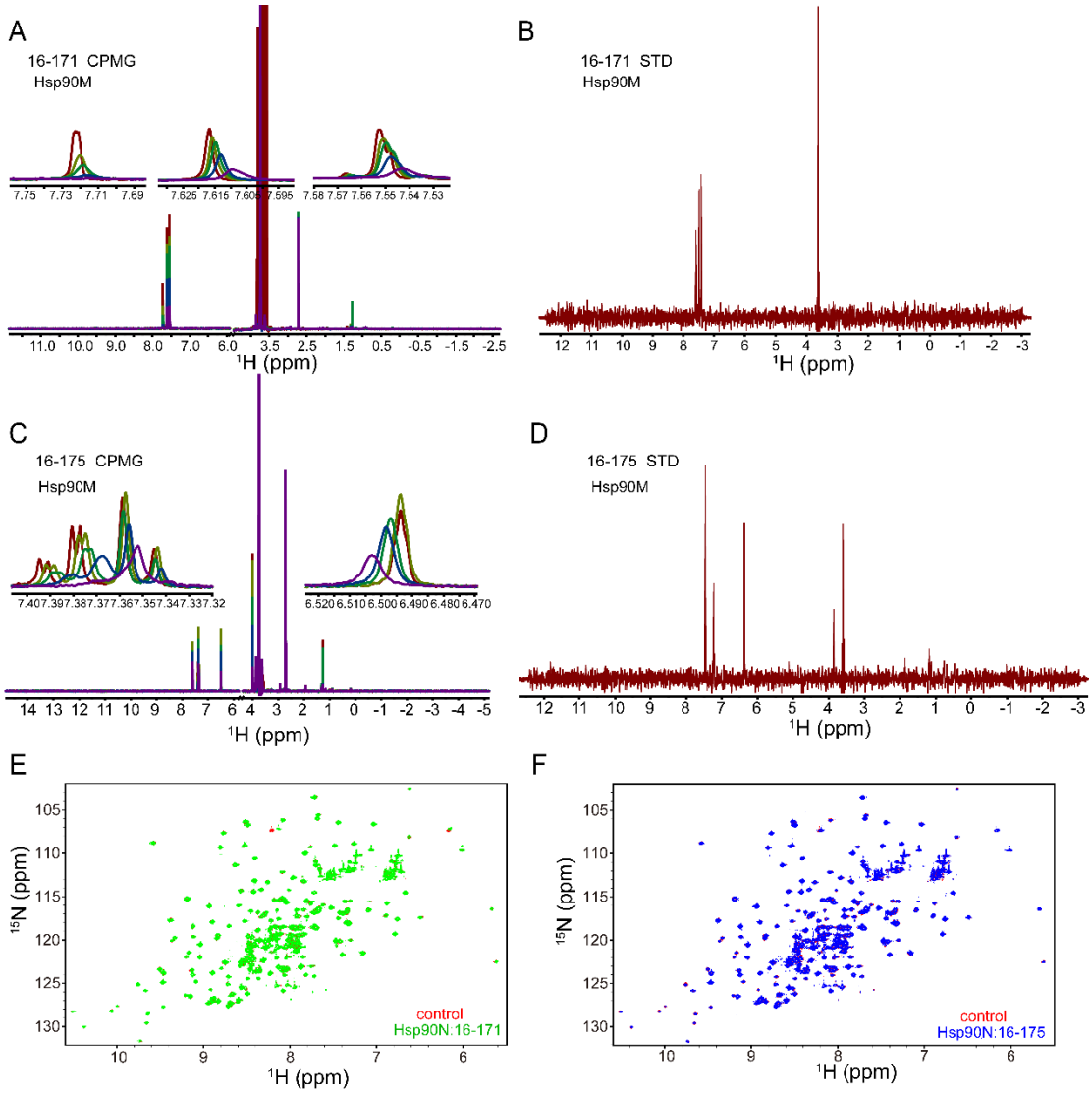

Figure S5. Ligand observed CPMG and STD spectra indicate that SOMCL-16-171 and SOMCL-16-175 directly interact with Hsp90α's middle domain. Related to Figure 2. (A) CPMG NMR spectra for **SOMCL-16-171** only (200 μM, red) and **SOMCL-16-171** (200 μM) in the presence of different concentrations of Hsp90α middle domain (2 μM, lime-green; 5 μM, green; 10 μM, blue; 20 μM, purple). (B) STD spectrum of **SOMCL-16-171** (200 μM) in the presence of Hsp90α middle domain (5 μM). (C) CPMG NMR spectra for **SOMCL-16-175** only (200 μM, red) and **SOMCL-16-175** (200 μM) in the presence of different concentrations of Hsp90α middle domain (2 μM, lime-green; 5 μM, green; 10 μM, blue; 20 μM, purple). (D) STD spectrum of **SOMCL-16-175** (200 μM) in the presence of Hsp90α middle domain (5 μM). (E) Superposition of [^{1}H, ^{15}N] HSQC spectra of Hsp90α's N-terminal domain without (red) and

with **SOMCL-16-171** (green, molar ratio of 1:4 Hsp90α N-terminal domain to **SOMCL-16-171**) reveals a non-significant spectral change upon the addition of the compound. (F) Superposition of [^{1}H, ^{15}N] HSQC spectra of Hsp90α's N-terminal domain without (red) and with **SOMCL-16-175** (blue, molar ratio of 1:4 Hsp90α N-terminal domain to **SOMCL-16-175**). No spectral change upon the addition of **SOMCL-16-175** was detected.

Figure S6

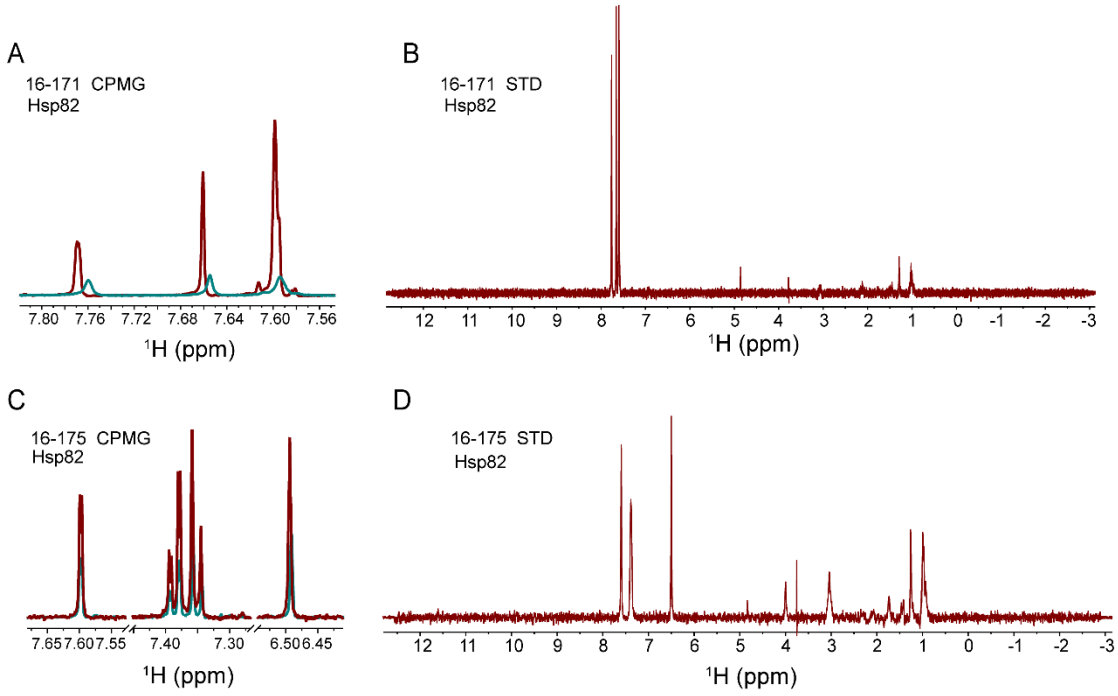

Figure S6. Ligand observed CPMG and STD spectra indicate that SOMCL-16-171 and SOMCL-16-175 directly interact with Hsp82 (Hsp90α yeast homolog). Related to Figure 2. (A) CPMG NMR spectra for **SOMCL-16-171** (200 μM, red) and **SOMCL-16-171** (200 μM) in the presence of Hsp82 (5 μM, green). (B) STD spectrum of **SOMCL-16-171** (200 μM) in the presence of Hsp82 (5 μM). (C) CPMG NMR spectra for **SOMCL-16-175** (200 μM, red) and **SOMCL-16-175** (200 μM) in the presence of Hsp82 (5 μM, green). (D) STD spectrum of **SOMCL-16-175** (200 μM) in the presence of Hsp82 (5 μM).

Figure S7

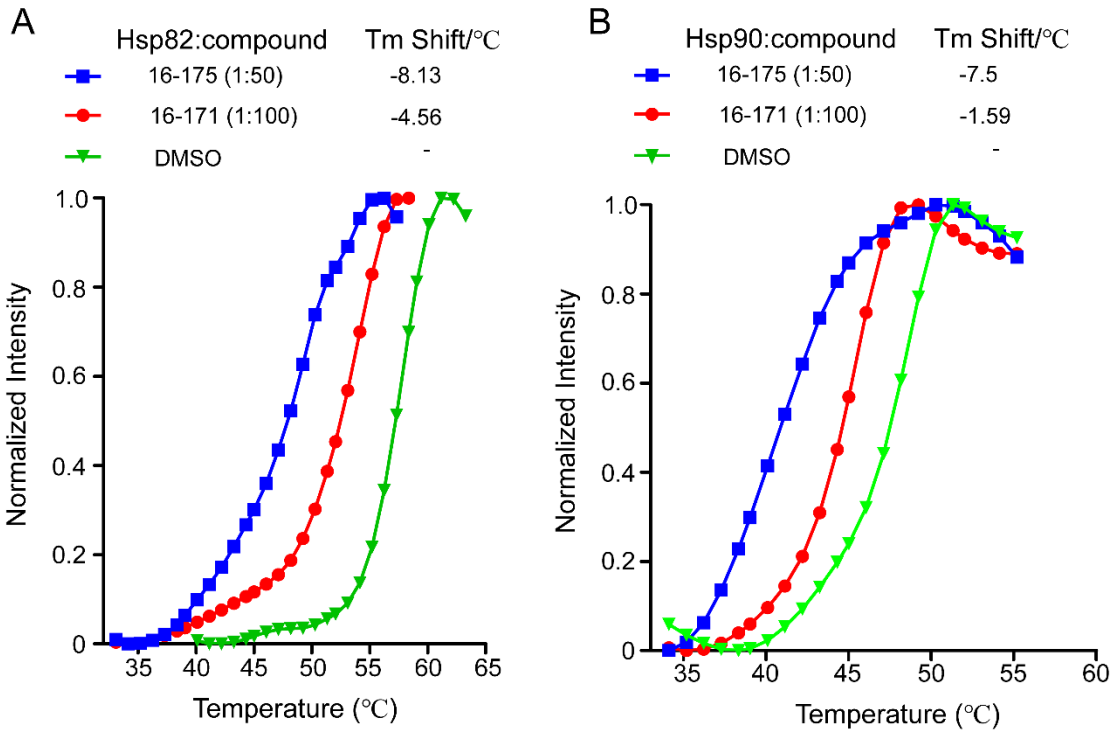

Figure S7. SOMCL-16-175 and SOMCL-16-171 directly interact with Hsp90α and its yeast homolog Hsp82. Related to Figure 3. (A, B) The shifts in *Tm* values of full-length Hsp90 (human Hsp90α), full-length Hsp82 (Hsp90α yeast homolog) upon the binding of **SOMCL-16-171** or **SOMCL-16-175** were determined.

Figure S8

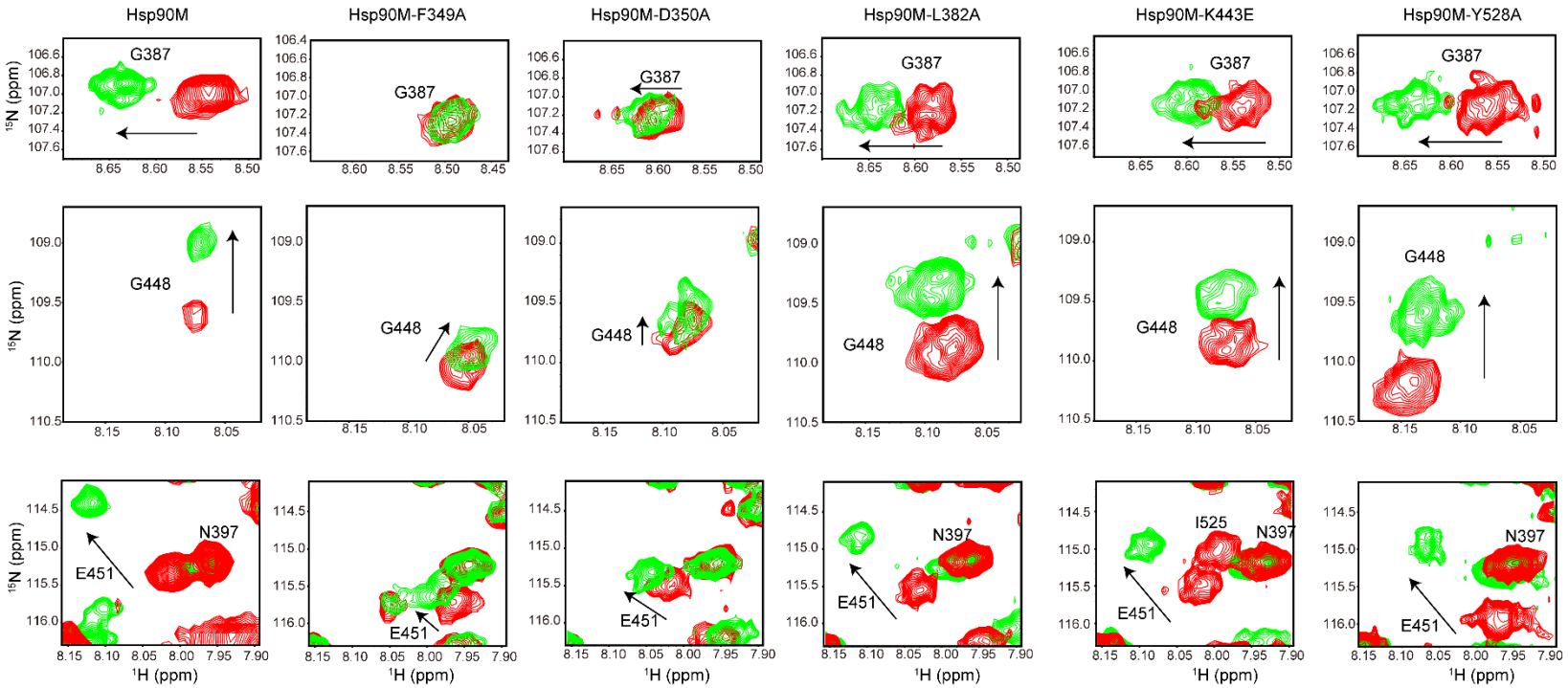

Figure S8. Compared with the wild-type chaperone, Hsp90M mutants with the mutation of representative residues potentially responsible for the recognition of active compounds present less significant or comparable chemical shift perturbations upon the addition of SOMCL-16-175. Related to Figure 4. Superposition of [^{1}H, ^{15}N] HSQC spectra of Hsp90M/Hsp90M-F349A/Hsp90M-D350A /Hsp90M-L382A/Hsp90M-K443E/Hsp90M-Y528A without (red) and with the presence of **SOMCL-16-175** (green, molar ratio of 1:6 Hsp90M or its mutants to **SOMCL-16-175**) reveals chemical shift perturbation effects upon active compound binding.

Figure S9

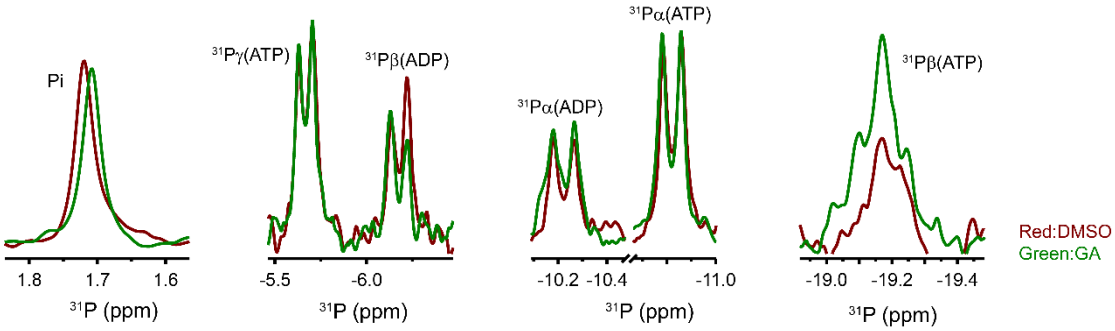

Figure S9. The ^{31}P NMR spectra data suggest that the application of Geldanamycin (known Hsp90 inhibitor binding to Hsp90's N-terminal domain) inhibits the ATPase activity of Hsp82. Related to Figure 4. The ATP hydrolysis process catalyzed by Hsp82 (Hsp90α yeast homolog) was monitored by acquiring 1D ^{31}P spectra at different reaction time points. Superposition of 1D ^{31}P spectra of Hsp82:ATP (3 μM:1mM) reaction system without (red) and with the presence of Geldanamycin (200 μM, green) acquired at the time point of 3 hours after the initiation of the reaction.

Figure S10

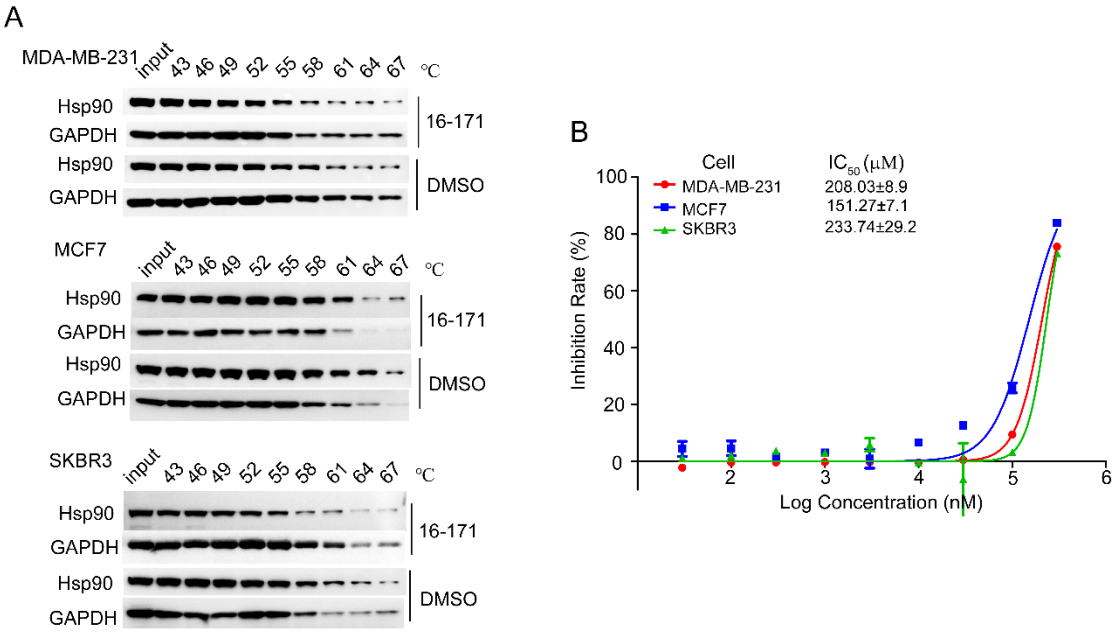

Figure S10. SOMCL-16-171 interacts with Hsp90 in cellular context and cause cytotoxicity in human breast cancer cell lines. Related to Figure 5. (A) Upon the treatment of **SOMCL-16-171**, decreased thermostability of Hsp90 in cellular context was observed. Extracts from MDA-MB-231, MCF7 and SKBR3 cells were used in the cellular thermal shift experiments. (B) Cell viability of MDA-MB-231, MCF7 and SKBR3 cells were assessed after exposure to vehicle, and different concentrations of **SOMCL-16-171** (30 nM, 100 nM, 300 nM, 1 μM, 3 μM, 10 μM, 30 μM, 100 μM, 300 μM) for 72 hours. Data are analyzed by GraphPad Prism 5 and presented as means ± S.D. (n = 3).

Figure S11

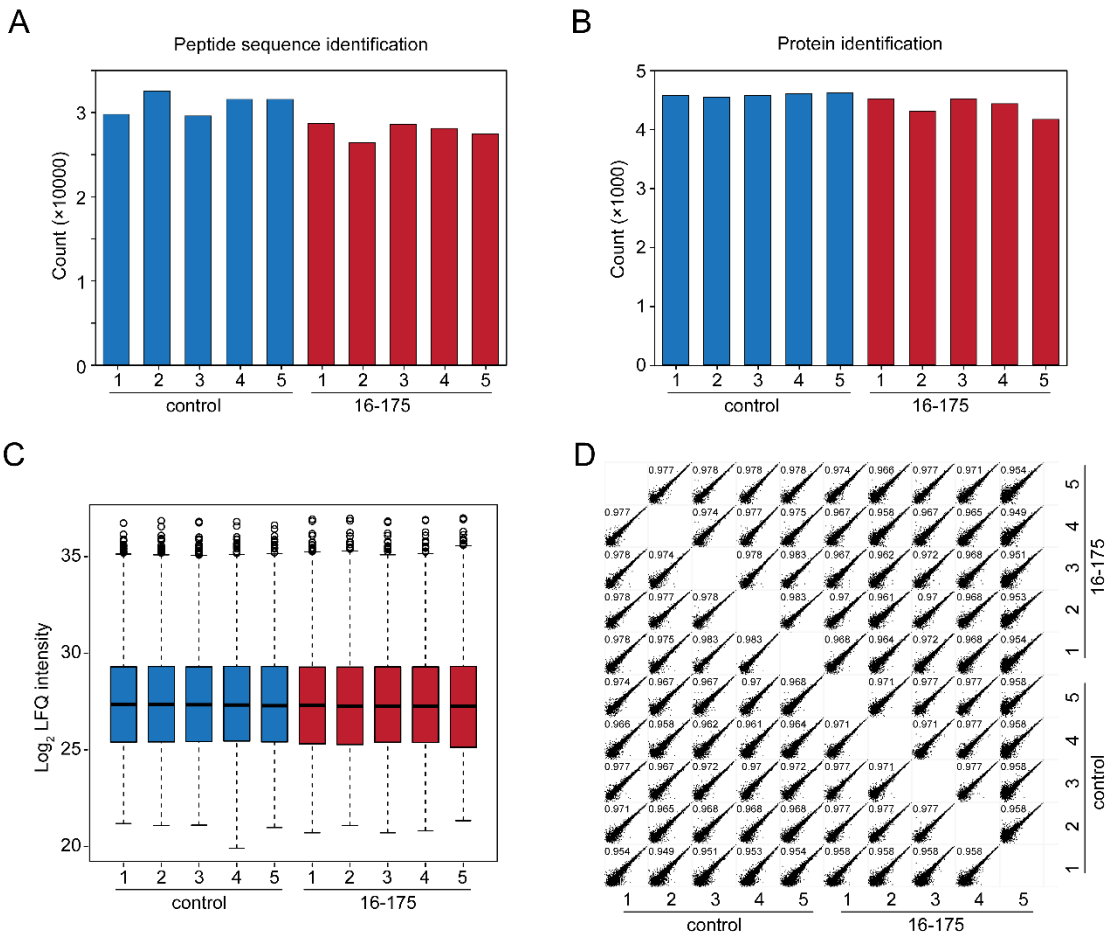

Figure S11. Summary of the proteomic data. Related to Figure 6. (A) Counts of peptide sequence identification. Totally, 51,393 peptide sequences were identified, with averagely ~30,000 in each sample. (B) Counts of protein identification. Totally, 4,866 proteins were identified, with averagely ~4,500 proteins in each sample. (C) Boxplot shows the distributions of log2-transformed LFQ intensities in each sample. (D) The quantification correlation plot. Pearson coefficients were calculated using all quantified proteins for each pair of samples.

Figure S12

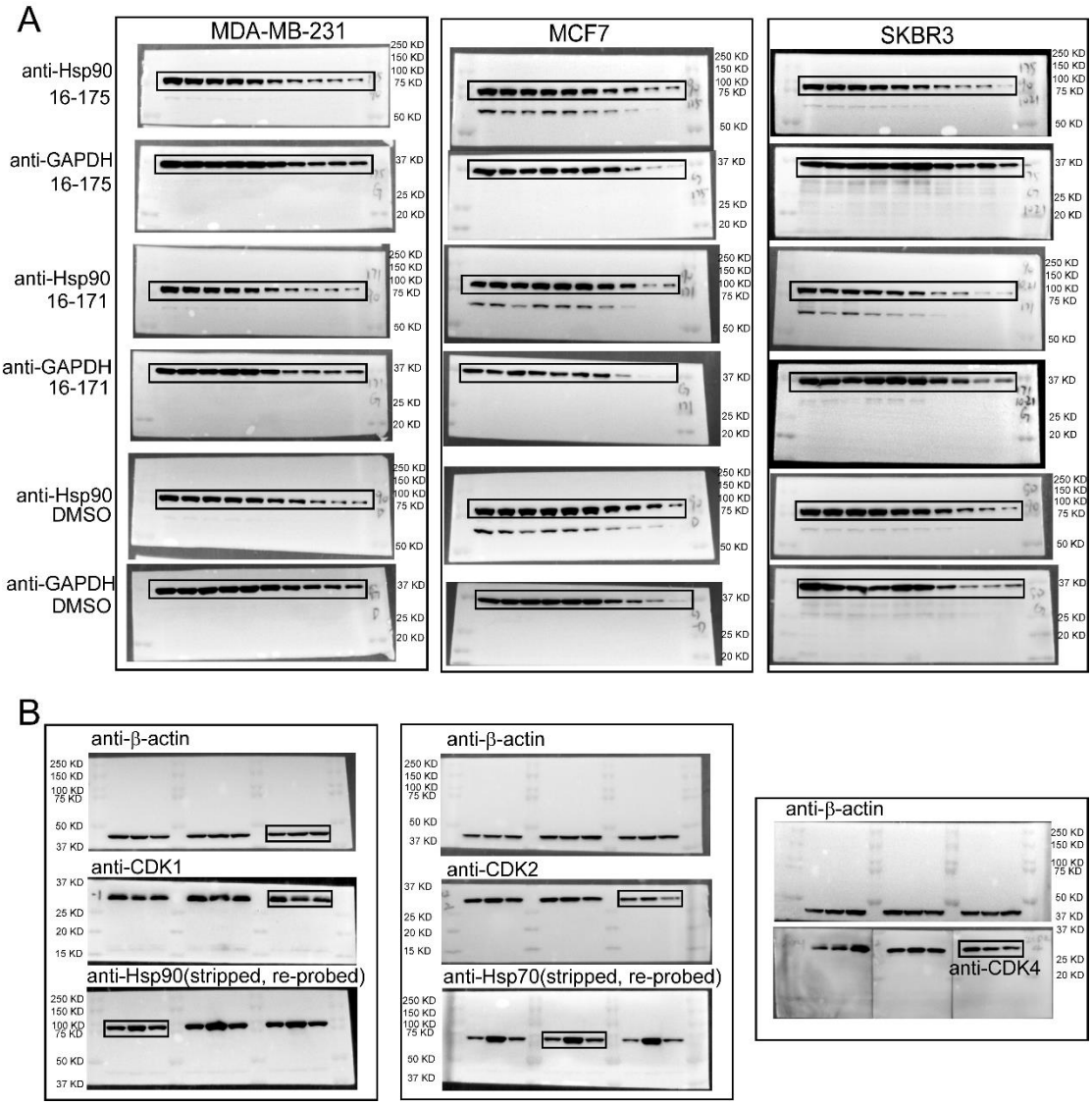

Figure S12. Uncropped western blot images shown in Figure 5A, supplemental Figure S10A and Figure 6E. (A) Related to Figure 5 and supplemental Figure S10. The cropped regions are framed. (B) Related to Figure 6. The cropped regions are framed.

Supplemental Table

Table S1

Table S1. Crystallography data collection and refinement statistics. Related to Figure 1.

PDB ID	6KSQ	**RMS values**	
Space group	*P*21	Bond length (Å)	0.008
Cell dimension: a (Å)	36.07	Bond angle (°)	0.867
b (Å)	38.97	**Numbers of non-hydrogen atoms**	
c (Å)	108.03	Protein	2094
Wavelength (Å)	0.979	Water Oxygen	62
Reflections (unique)	14524	Others	0
Resolution range (Å)	2.20-36.64	**Mean temperature factors (Å^2)**	
Highest-resolution shell (Å)	2.20-2.24	Protein	45.35
Redundancy	6.30	**Ramachandran plot**	
I/σ (I)	8.50	Favored (%)	98.41
Completeness (%)	94.50	Allowed (%)	1.59
Rwork/Rfree	0.182/0.232	Outliers (%)	0.00

Synthesis of compound SOMCL-16-171 and SOMCL-16-175

Synthesis of compound SOMCL-16-171

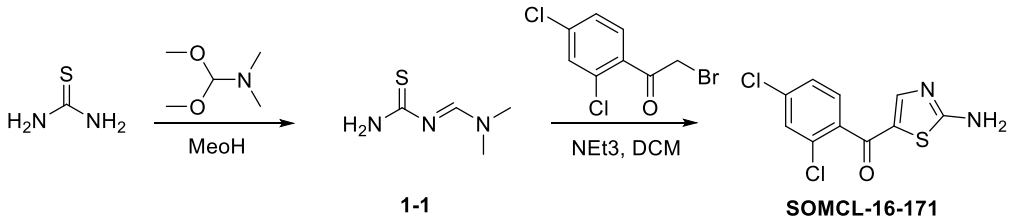

(E)-*N′*-Carbamothioyl-*N*,*N*-dimethylformimidamide (1-1):

To a solution of thiourea (760 mg, 10 mmol) in menthol was added N,N-dimethylformamide dimethyl acetal (1.3 equiv). The mixture was heated at 80 °C for 4 h. Then the mixture was concentrated and purified with column chromatography to afford the title compound as light yellow solid in 46%. **^{1}H NMR** (300 MHz, $CDCl_3$) δ 8.78 (s, 1H), 3.75 (m, 2H), 3.21 (s, 3H), 3.10 (s, 3H).

(2-Aminothiazol-5-yl)(2,4-dichlorophenyl)methanone (SOMCL-16-171):

To a solution of **1-1** (200 mg, 1.527 mmol) in CH_2Cl_2 were added 2-bromo-1-(2,4-dichlorophenyl)ethanone (1 equiv) and triethylamine (2 equiv). The mixture was stirred at room temperature overnight. Then the mixture was concentrated, and the residue obtained was purified with column chromatography to yield **SOMCL-16-171** as yellow solid in 40%. **^{1}H NMR** (300 MHz, $CDCl_3$) δ 7.50 (s, 1H), 7.40 – 7.31 (m, 3H), 6.06 (s, 2H); **^{13}C NMR** (151 MHz, $CDCl_3$) δ 184.39, 174.80, 151.23, 136.67, 136.28, 132.29, 130.26, 129.78, 129.75, 127.01; **ESI-MS**: 271 $[M - H]^+$; **HRMS-ESI**: *m/z* $[M - H]^+$ calcd for $C_{10}H_5Cl_2N_2OS$: 270.9500, found: 270.9508.

Synthesis of compound SOMCL-16-175

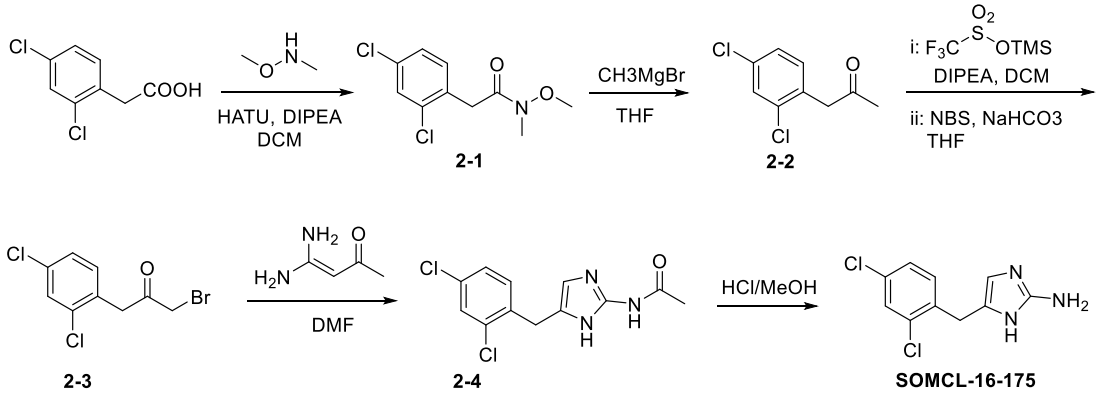

2-(2,4-Dichlorophenyl)-*N*-methoxy-N-methylacetamide (2-1):

To a solution of 2-(2,4-dichlorophenyl)acetic acid (205 mg, 1 mmol) in CH_2Cl_2 were added N,O-dimethylhydroxylamine (1.3 equiv), 1-(3-dimethylaminopropyl)-3-ethylcarbodiimide hydrochloride (EDCI, 1.3 equiv) and 1-hydroxybenzotriazole (HOBT, 1.3 equiv). Di(isopropyl)ethylamine (DIPEA, 3 mL) was added. The mixture was stirred at room temperature for 2 h, and then concentrated. The residue was purified with column chromatography to yield the title compound as colorless oil in 80% yield. **^{1}H NMR** (300 MHz, $CDCl_3$) δ 7.39 (s, 1H), 7.25–7.18 (m, 2H), 3.87 (s, 2H), 3.71 (s, 3H), 3.21 (s, 3H).

1-(2,4-Dichlorophenyl)propan-2-one (2-2):

A solution of **2-1** (197 mg, 0.798 mmol) in THF cooled to -78 ºC was added to the solution of N-acetylguanidine (0.86 mL, 1.4 M) in MeOH/toluene. The mixture was stirred at -78 °C for 30 min, followed by stirring at room temperature for 1 h. The reaction was quenched with saturated aqueous NH_4Cl solution, extracted with ethyl acetate, concentrated and purified with column chromatography to yield the title compound as colorless oil in 77% yield. **^{1}H NMR** (300 MHz, $CDCl_3$) δ 7.41 (s, 1H), 7.22 (d, J = 8.2 Hz, 1H), 7.14 (d, J = 8.2 Hz, 1H), 3.82 (s, 2H), 2.22 (s, 3H).

1-Bromo-3-(2,4-dichlorophenyl)propan-2-one (2-3):

DIPEA (1.2 equiv) and trimethylsilyl trifluoromethanesulfonate (1.1 equiv) were added to the solution of **2-2** (33 mg, 0.118 mmol) in CH_2Cl_2 at -78 ºC and stirred for 1h. The reaction was then quenched with saturated aqueous $NaHCO_3$ solution, extracted with CH_2Cl_2 and concentrated. The residue was dissolved in THF. $NaHCO_3$ (1.2 equiv) and NBS (1.2 equiv) were added sequentially at 0 ºC. The mixture was warmed to room temperature and stirred overnight. After removal of the solvents, the residue was purified with column chromatography to yield the title compound as yellow solid in 19% yield. **^{1}H NMR** (300 MHz, $CDCl_3$) δ 7.42 (d, J = 1.5 Hz, 1H), 7.23 (d, J = 1.7 Hz, 1H), 7.18 (d, J = 8.2 Hz, 1H), 4.07 (s, 2H), 3.98 (s, 2H).

***N*-(5-(2,4-Dichlorobenzyl)-1H-imidazol-2-yl)acetamide (2-4):**

A solution of **2-3** (33 mg，0.118 mmol) in DMF at 0 ºC was added the solution of N-acetylguanidine (2 equiv) in CH_2Cl_2 (1 mL). The mixture was stirred at room temperature overnight. Then water was added, and the mixture and was extracted with ethyl acetate, washed

with brine, and dried over $MgSO_4$. After filtration and concentration, the residue obtained was purified with column chromatography to yield the title compound as yellow solid in 27% yield. **^{1}H NMR** (300 MHz, $CDCl_3$) δ 7.39 (s, 1H), 7.15 (d, J = 8.0 Hz, 2H), 6.44 (s, 1H), 3.96 (s, 2H), 2.17 (s, 3H).

5-(2,4-Dichlorobenzyl)-1H-imidazol-2-amine (SOMCL-16-175):

A solution of **2-4** in HCl/MeOH was stirred at 60 °C overnight. The mixture was then concentrated and the residue was purified with column chromatography to yield **SOMCL-16-175** as brown oil in 18% yield. **^{1}H NMR** (300 MHz, $CDCl_3$) δ 7.33 (s, 1H), 7.18 (t, J = 7.8 Hz, 2H), 6.15 (s, 1H), 4.45 – 4.19 (m, 2H), 3.83 (s, 2H); **^{13}C NMR** (126 MHz, $CDCl_3$) δ 147.62, 134.62, 133.84, 132.89, 131.49, 129.53, 127.56, 124.19, 109.33, 29.71; **ESI-MS**: 242 $[M + H]^+$; **HRMS-ESI**: *m/z* $[M + H]^+$ calcd for $C_{10}H_{10}Cl_2N_3$: 242.0252, found: 242.0246.

^{1}H, ^{13}C-NMR spectra of SOMCL-16-171 and SOMCL-16-175

^{1}H, ^{13}C-NMR spectra of SOMCL-16-171

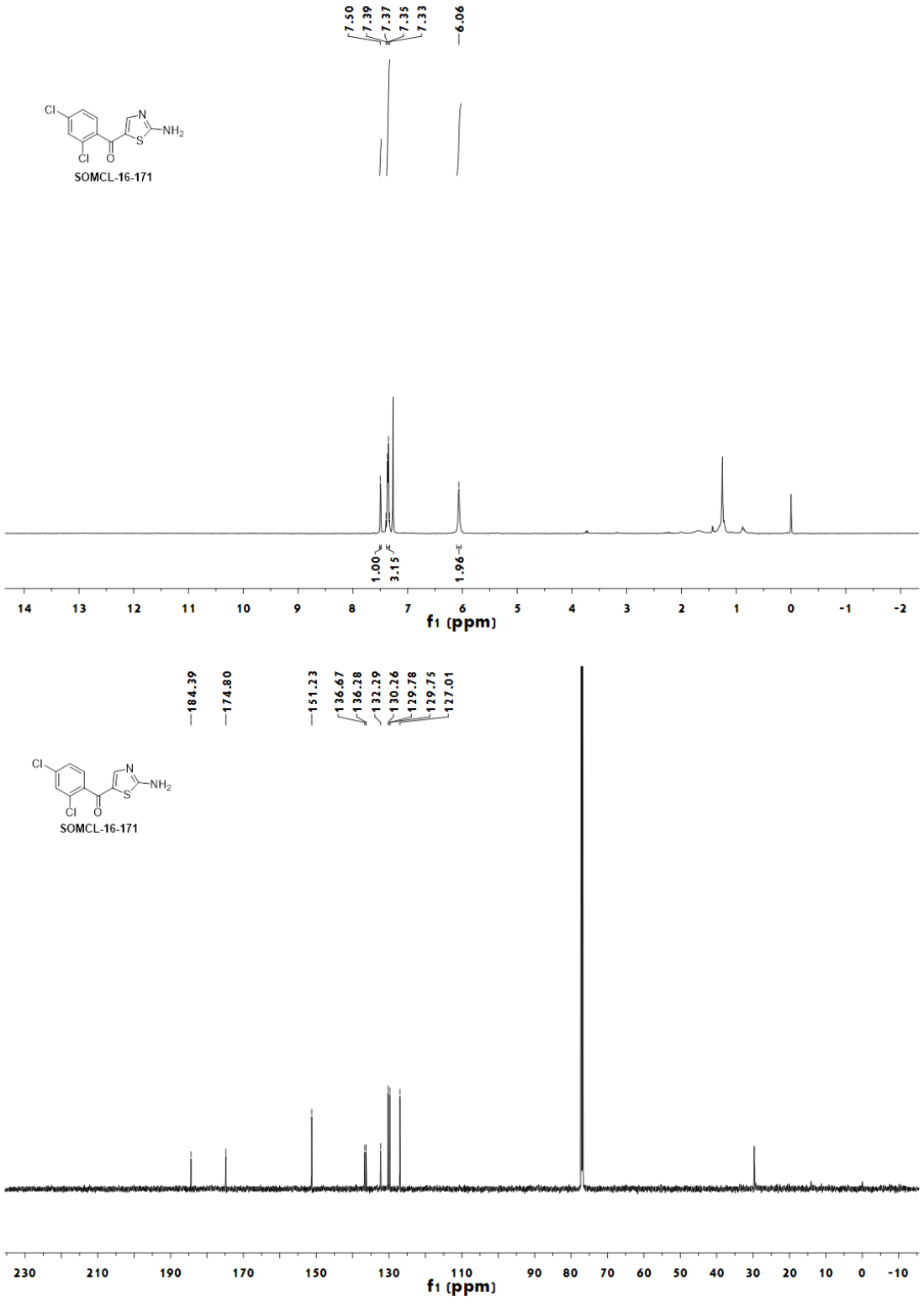

^{1}H, ^{13}C-NMR spectra of SOMCL-16-175

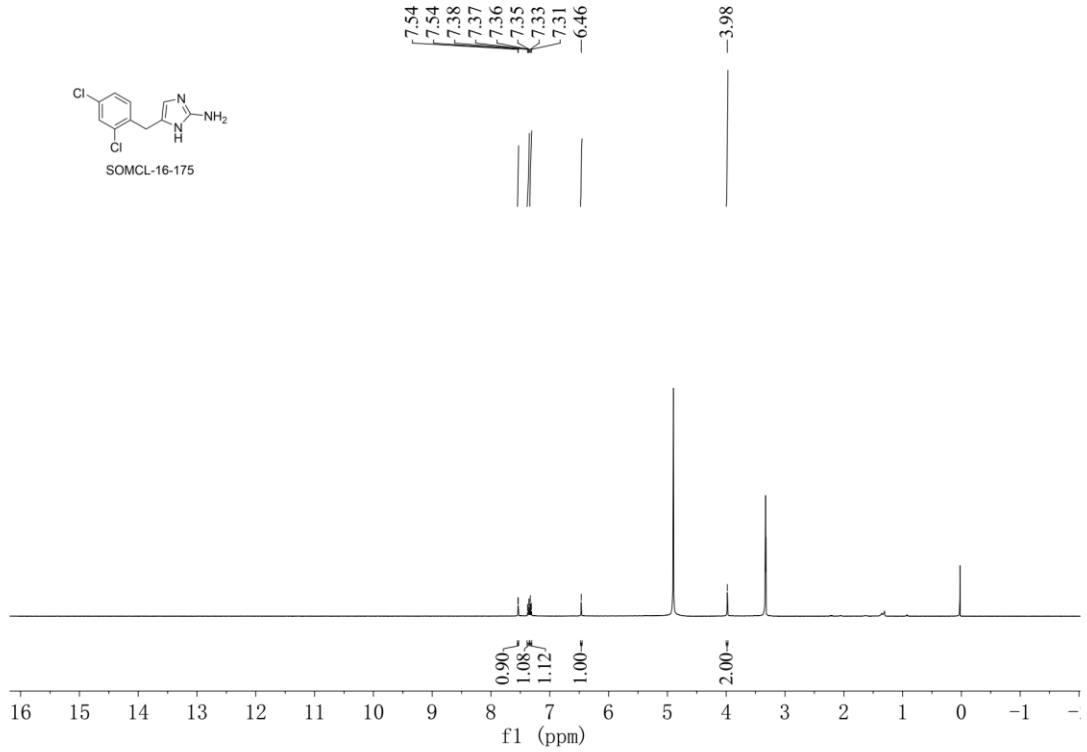

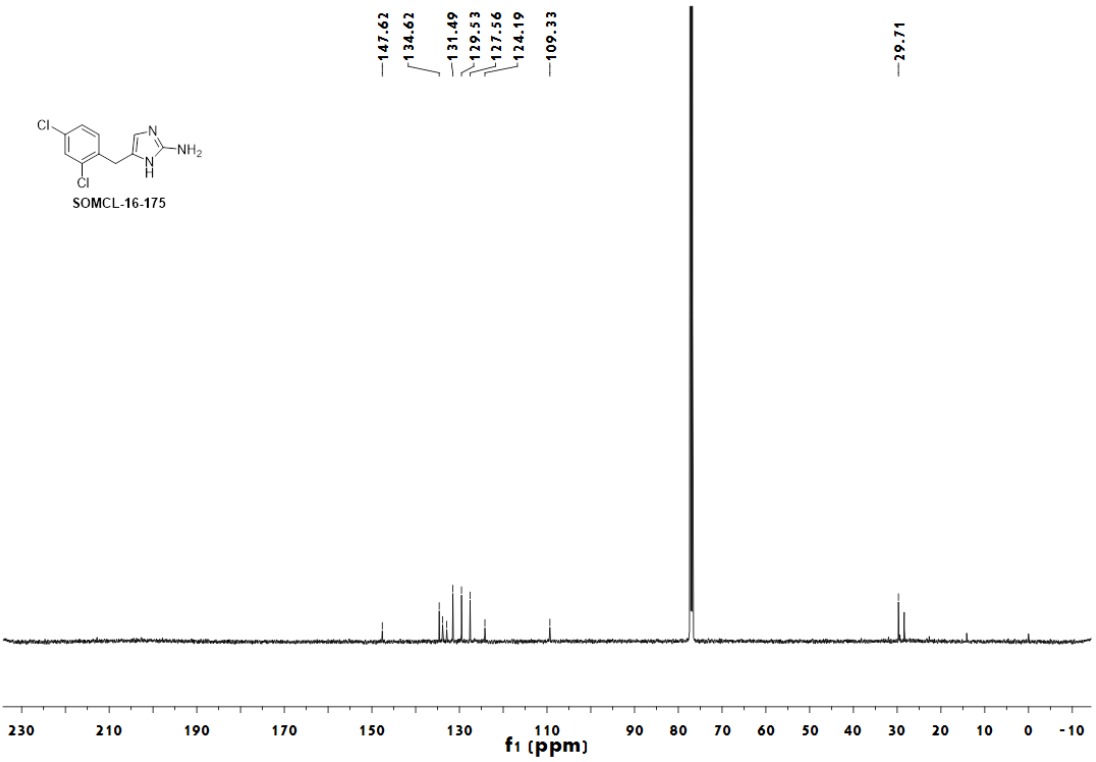

Transparent Methods

Protein sample preparation

Full-length cDNA of Hsp90α and Hsp82 were kindly provided by Dr. Liguang Lou (Shanghai Institute of Materia Medica, Chinese Academy of Sciences, China). $Hsp90^{9-236}$ (Hsp90N) plasmid was a gift from Dr. Jianhua He (National Facility for Protein Science in Shanghai, ZhangJiang Lab, China). Wide-type Sortase A^{60-206} expression plasmid was a gift from Dr. Caiguang Yang (Shanghai Institute of Materia Medica, Chinese Academy of Sciences, China). $Hsp90^{293-554}$ (Hsp90M), $Hsp90^{9-240}$LPKTG, $Hsp90^{273-554}$ and $Hsp90^{9-554\Delta241-268}$ (Hsp90 NMΔ) were sub-cloned into pET28a or pET15b vector. The mutants for $Hsp90^{293-554}$ and Sortase A^{60-206} (P94S/D160N/K196T) were created by PCR.

His-tagged $Hsp90^{9-236}$, $Hsp90^{293-554}$, $Hsp90^{293-554}$ mutants, $Hsp90^{9-554\Delta241-268}$, Hsp90, Hsp82, $Hsp90^{9-240}$LPKTG, $Hsp90^{273-554}$ and Sortase A^{60-206} (P94S/D160N/K196T) were expressed in *Escherichia coli* and purified by using a combination of affinity chromatography and size exclusion chromatography on an FPLC system. $Hsp90^{273-554}$ was cleaved from its His-tag during elution from Ni-NTA resin by using thrombin. Hsp90 NMΔ with its N-terminal domain isotope labelled was prepared by following the reported protocol with a moderate modification (Freiburger et al., 2015). Hsp90 NMΔ with its N-terminal domain isotope labelled was synthesized by using two protein samples $Hsp90^{9-240}$LPKTG and $Hsp90^{273-554}$. $Hsp90^{9-240}$LPKTG and $Hsp90^{273-554}$ that were selectively labelled or unlabelled were incubated with Sortase A^{60-206} (P94S/D160N/K196T) at 20 ℃ for 80 minutes. The molar ratio of $Hsp90^{9-240}$LPKTG:$Hsp90^{273-554}$:Sortase A^{60-206} (P94S/D160N/K196T) for the protein ligation reaction is 1:2:2. To inhibit the reverse process of the ligation, protein concentrator with a molecular weight cutoff at 10 kDa was used as the container and centrifuged at 2000 × *g* during the reaction to remove the peptide byproduct. The Hsp90 NMΔ formed was subsequently purified by using a HiTrap Q HP column, followed by size exclusion chromatography. ^{15}N, ^{13}C, and ^{2}H labelled samples were produced by growth in M9 minimal media with ^{15}N labelled ammonium chloride, ^{13}C labelled glucose, and D_2O used as the nitrogen, carbon, and water sources, respectively.

NMR spectroscopy

All triple resonance experiments including HNCA, HN(CO)CA, HNCO, HN(CA)CO, HNCACB and CACB(CO)NH were recorded with ^{15}N, ^{13}C and 70% deuterium triple-labelled $Hsp90^{293-554}$ on Bruker 600 MHz NMR spectrometer equipped with a cryogenically cooled probe at 20 ℃. [^{1}H, ^{15}N] HSQC spectra were acquired on Bruker 600 MHz or 900 MHz NMR spectrometers equipped with a cryogenically cooled probe at 20 ℃. 1D ^{31}P spectra were acquired on Bruker 500 MHz NMR spectrometer equipped with a liquid nitrogen cooled cryoprobe at 25 ℃. The spectra were processed by using NMRPipe (Delaglio et al., 1995) and analyzed with CARA (Keller, 2004) and Sparky (Kneller and Kuntz, 1993). Chemical shift perturbation values ($\Delta\delta_{avg}$) for ^{15}N and ^{1}H nuclei were derived from the following equation:

$$\Delta\delta_{avg} = \sqrt{\left((\Delta\delta_N/5)^2 + \Delta\delta_H{}^2\right)/2}$$

where $\Delta\delta_N$ and $\Delta\delta_H$ represent the observed chemical shift changes in dimension ^{15}N and ^{1}H dimension, respectively. Based on the protein concentrations and the CSP values provided by the NMR titration experiments of ^{15}N-labelled Hsp90M and **SOMCL-16-175**, dissociation constant (K_d) was determined by global fitting according to the equation below:

$$\Delta\delta_{avg} = \frac{\delta_{TOT}\left(nL_T + nP_T + K_d - \sqrt{(nL_T + nP_T + K_d)^2 - 4n^2L_TP_T}\right)}{2nP_T}$$

where $\Delta\delta_{avg}$ donates the observed chemical shift change, δ_{TOT} is the chemical shift difference between free and complexed protein, n is the binding stoichiometry, L_T is the concentration of titrant protein and P_T is the total concentration of analyte protein (Fielding, 2007).

Crystal structure determination

Crystals of Hsp90α's middle domain were obtained by using hanging drop vapor diffusion method in a solution containing 0.5 M ammonium sulfate, 29.5% (w/v) polyethylene glycol 3350 and 5% glycerol (pH 8.5) at 4 ℃. The final concentration of Hsp90M used in the crystallization was 0.12 mM. The crystals obtained were cryo-protected in the crystallization buffer containing 20% (v/v) glycerol and flash cooled in liquid nitrogen. X-ray diffraction data were collected at beamline BL17U1 at the Shanghai Synchrotron Radiation Facility (Wang et al., 2018). The data were processed with HKL3000 (Minor et al., 2006). The structure was

solved by molecular replacement using the program CCP4 with a search model of PDB code 1HK7 (Bailey, 1994; Meyer et al., 2003). The models were built using coot and refined with a simulated-annealing protocol implemented in the program PHENIX (Adams et al., 2002; Emsley and Cowtan, 2004). Data collection and refinement statistics of the solved structure was shown in Table S1.

Fragment-based active compound discovery

Hit fragment compound screening with Hsp90α's middle domain as the target were carried out by following our previously reported protocol (Yu et al., 2016). In the first round of screening, 200 μM grouped fragment compound mixtures without or with the presence of 5 μM Hsp90M were dissolved in phosphate buffer (20 mM NaH_2PO_4/Na_2HPO_4, 100 mM NaCl and 2% DMSO in D_2O) and used in ligand-observed CPMG and STD spectrum acquisition. The potential hit compound candidates were then subjected to a second-round of screening by using CPMG and STD NMR experiments. 200 μM single potential hit compound without or with the presence of 5 μM Hsp90M were used in the second-round of screening. All of the ligand observed CPMG and STD NMR experiments were acquired at 25 °C on Bruker 600 MHz NMR spectrometer equipped with a cryogenically cooled probe.

*General synthetic approach for **SOMCL-16-171** and **SOMCL-16-175***

The general synthetic approach for compounds is summarized in scheme 1. The synthesis of **SOMCL-16-171** commenced from the condensation of thio-urea with DMF-DMA followed by cyclization with 2-bromo-1-(2,4-dichlorophenyl)ethanone. The synthesis of **SOMCL-16-175** was started from 2-(2,4-dichlorophenyl)acetic acid, which was first transformed to the ketone intermediates **2-2** through forming the Weinreb amide **2-1** followed by treatment with Grignard reaction. Subsequent bromination of **2-2** gave intermediate **2-3**, which was then subjected to cyclization with N-acetylguanidine and removal of acetyl under acidic condition to yield compound **SOMCL-16-175**.

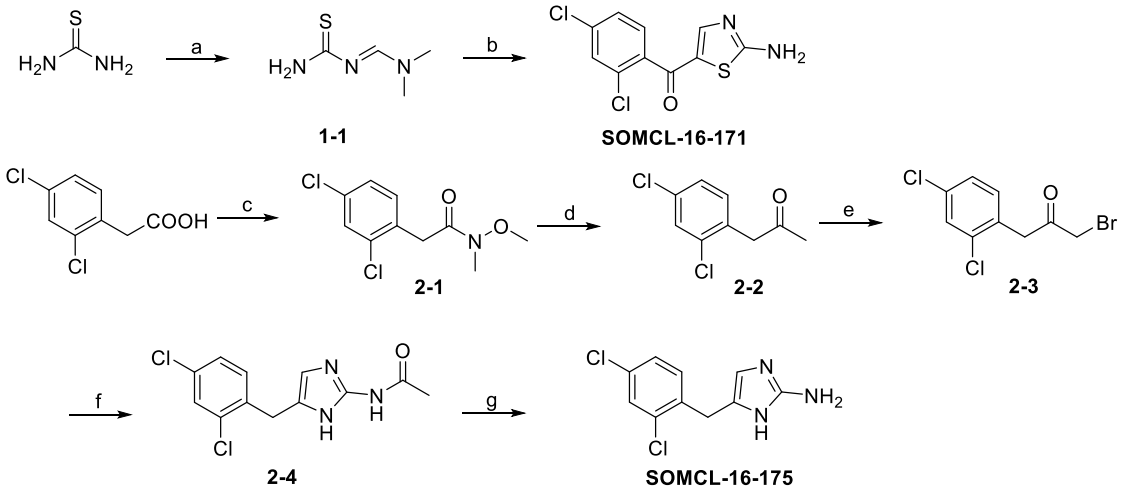

Scheme 1. Synthetic route of **SOMCL-16-171** and **SOMCL-16-175.** Reagents and conditions：(a) N,N-Dimethylformamide dimethyl acetal, MeOH, reflux, 46%; (b) 2-bromo-1-(2,4-dichlorophenyl)ethanone, Triethylamine, DCM, rt, 40%; (c) N,O-dimethylhydroxylamine for 6-22, 2,4-dichloroaniline for 6-37, HATU, HOAT, DIPEA, DCM, rt, 73-80%; (d) CH3MgBr, THF, -78℃~0℃, 77%; (e) (i) Trimethylsilyl trifluoromethanesulfonate, DIPEA, -78℃; (ii) NBS, NaHCO3, THF, 0℃~60℃, 19% (two steps); (f) N-acetylguanidine, DMF, 0℃~60℃, 27%; (g) HCl/MeOH, 60℃, 18%.

Molecular docking

The crystal structure of Hsp90α's middle domain (PDB: 6KSQ) was prepared using the Protein Preparation Wizard implemented in the Schrödinger suite (Sastry et al., 2013). This procedure added hydrogen atoms and missing side chains of residues. The orientation of polar hydrogens and the protonated states of the receptor were then optimized. The overall structure was refined using OPLS3 force field (Harder et al., 2016) with harmonic restraints on heavy atoms. The 3D structure of **SOMCL-16-175** was generated and optimized using the Ligprep tool of the Schrödinger suite, and the docking of **SOMCL-16-175** to Hsp90M was performed with the Induced Fit Docking (IFD) tool. The detailed protocol of IFD tool can be found as previously published (Koldso et al., 2010). The docking grid was centered on the centroid of eight residues: Phe349, Leu363, Asp372, Gly387, Lys 443, Glu451, Ile522, and Glu535. These residues were chosen according to the NMR studies. The following docking simulation was performed with default settings except that the extra precision (XP) mode was used in the last docking round. The final pose was selected from the top-scoring conformations.

Isothermal titration calorimetry measurements

All ITC measurements were performed at 30 ℃ by iTC200 calorimeter (GE Healthcare) in an ITC buffer (20 mM Tris, 75 mM NaCl, 6 mM $MgCl_2$ and 1 mM β-mercaptoethanol, pH 7.4) while stirring at 800 rpm. Hsp90 NMΔ protein samples were premixed with DMSO or either with one of two compounds (ten-fold molar excess of **SOMCL-16-171** or **SOMCL-16-175**). Pretreated protein was diluted with the ITC buffer to 50 μM, and ADP or AMPPNP was diluted with the ITC buffer to a final concentration of 1 mM. The final concentration of DMSO in the reaction buffer is 2.5% of the total volume. The titrations were performed using an initial injection of 0.4 μL followed by 19 identical injections of 2 μL ADP or AMPPNP to the cell, and last three data points were averaged to account for the heat of dilution. Data were analyzed by using the program Origin 7.0.

Thermal shift assay

Protein thermal shift experiments were performed on a 7500 fast real-time PCR system (ABI, United States). Each reaction system contains 5 × SYPRO Orange, 10 μM protein sample and 1 mM **SOMCL-16-171** or 500 μM **SOMCL-16-175** dissolved in 20 μL of thermal shift assay buffer (20 mM Tris, 75 mM NaCl and 1 mM β-mercaptoethanol, pH 7.4). The mixture samples were heated from 25 ℃ to 99 ℃ at 1% Ramp rate, and the melting curves were processed by using Protein Thermal Shift software 1.3.

ATP hydrolysis assay

The ATP hydrolysis process catalyzed by Hsp82 (Hsp90α yeast homolog) was monitored by recording ^{31}P NMR spectra on Bruker 500 MHz NMR spectrometer equipped with a liquid nitrogen cooled cryoprobe at 25 ℃. The reaction systems containing 3 μM Hsp82 and 1 mM ATP without or with the presence of 500 μM **SOMCL-16-175** or 200 μM Geldanamycin (GA) were dissolved in reaction buffer (100 mM Tris, 20 mM KCl, 6 mM $MgCl_2$, pH 7.4) and incubated at 37 ℃. The ^{31}P NMR spectra were acquired right after a three hour incubation.

Cellular thermal shift assay（CETSA）

Cellular thermal shift assay was conducted according to the protocol as reported (Molina et al., 2013). MDA-MB-231, MCF7 and SKBR3 cells were harvested with PBS buffer and lysed by subjecting to three freeze-thaw cycles. Then, the cell lysates were mixed and incubated

with **SOMCL-16-175** (500 μM) or **SOMCL-16-171** (1 mM) or DMSO (1 %) at room temperature for 20 minutes. After pre-incubation the mixture samples were divided into aliquots and submitted to a paralleled incubation at different temperatures ranging from 43 ℃ to 67 ℃ lasting for 5 minutes. Finally, the denatured samples were centrifuged, and the supernatants were analyzed by immunoblotting.

Cell viability and colony formation assays

Breast cancer cells MDA-MB-231, MCF7, and SKBR3 were cultured in DMEM/F12, DMEM, and RPMI 1640 medium, respectively. 10% fetal bovine serum was added into the medium during cell culturing. To test the effects of **SOMCL-16-171** and **SOMCL-16-175** on the viability of breast cancer cell lines, 4000 cells/well MDA-MB-231, 6000 cells/well MCF7, and 6000 cells/well SKBR3 were seeded to 96-well flat-bottomed microtiter plates and treated with DMSO or different concentrations of compounds (30 nM, 100 nM, 300 nM, 1 μM, 3 μM, 10 μM, 30 μM, 100 μM, 300 μM) for 72 h. The cell viability were then determined by Sulforhodamine B (S1402, Sigma) assay. The absorbance at 510 nm was measured in SpectraMax M5 (Molecular Devices), and the obtained data were analyzed by using GraphPad Prism 5.

The colony formation assays were performed using MDA-MB-231, MCF7, and SKBR3 cells with or without the treatment of **SOMCL-16-175**. 500 cells/well were plated in six-well plates and treated with either the compound (7.5 μM for MDA-MB-231 and SKBR3 cells, 17.5 μM for MCF7 cells) or 0.1% DMSO for about 7-15 days. The cell colony was fixed by using methyl alcohol, and then tinted using 0.5% crystal violet. Colony numbers were counted in Adobe Photoshop CS5.

Sample preparation and LC-MS/MS data acquisition for proteomics study

MCF7 cells were cultured and then treated by 0.1% DMSO or 35 μM **SOMCL-16-175** for 48 h. Cells were lysed with SDS lysis buffer (100-mM dithiothreitol, 4% sodium SDS, 100-mM Tris-HCl, pH 7.6). Proteins were extracted by ultrasonication (15% amplitude, 5s on and 5s off for 1 min, JY92-IIDN, Ningbo Scientz Biotechnology Co., LTD, China) and then denatured and reduced at 95°C for 5 min. Protein concentration was determined by a tryptophan-based fluorescence quantification method. The filter-aided sample preparation

(FASP) method was used for digesting proteins. Briefly, 50 μg proteins were loaded in a 10 kDa centrifugal filter tube (Millipore), washed twice with 200 μL UA buffer (8 M urea in 0.1 M Tris-HCl, pH 8.5), alkylated with 50 mM iodoacetamide in 200 μL UA buffer for 30 min in the darkness, washed thrice with 100 μL UA buffer again and finally washed thrice with 100 μL 50 mM NH_4HCO_3. All above steps were centrifuged at 12,000 g at room temperature. Proteins were digested by trypsin (1:50 of w/w, Promega Corporation, Madison, WI, USA) at 37°C for 16 h, and peptides were collected by centrifugation. Digested peptides were purified using C18 Stage-tips and evaporated to dryness in a Speed-Vac sample concentrator. Finally, ~2 μg peptides were subjected to LC-MS/MS analysis for each sample.

Peptides were separated and analyzed by coupling an Easy nano-UPLC1200 liquid chromatography (Thermo Fisher Scientific) to a Q Exactive HF mass spectrometer (Thermo Fisher Scientific). Peptides were loaded on to an in-house packed analytical column (75 μm i.d. × 30 cm, ReproSil-Pur C18-Pur, 1.9 μm, Dr. Maisch GmbH, Ammerbuch, Germany), with a 180-min gradient at a flow rate of 300 nL/min. The column was heated to 55°C using a column compartment to prevent overpressure during LC separation. Mobile phase A consisted of 0.1% formic acid, and mobile phase B consisted of 0.1% formic acid in 80% acetonitrile. The gradient was set as follows: 2%-5% B in 1 min; 5%-33% B in 145 min; 33%-45% B in 22 min; 45%-100% B in 4 min; 100% B in 8 min. The spray voltage was set at 2,300 V in positive ion mode and the ion transfer tube temperature was set at 300 °C. Data-dependent acquisition was performed using Xcalibur software in profile spectrum data type. The MS1 full scan was set at a resolution of 60,000 @ m/z 200, AGC target 3e6 and maximum IT 20 ms by orbitrap mass analyzer (350-1700 m/z), followed by 'top 20' MS2 scans generated by HCD fragmentation at a resolution of 15,000 @ m/z 200, AGC target 1e5 and maximum IT 100 ms. Isolation window was set at 1.6 m/z. The normalized collision energy (NCE) was set at NCE 27%, and the dynamic exclusion time was 40 s. Precursors with charge 1, 7, 8 and >8 were excluded for MS2 analysis.

Proteomics data analysis

All mass spectrometric data were analyzed using MaxQuant 1.6.5.0 against the human Swiss-Prot database containing 20,231 sequences (downloaded in December, 2017). Label-free

quantification (LFQ) was chosen for proteomic quantification using the default parameters. The function of "Match between runs" was used to reduce missing values in proteome quantification with a matching time window of 0.7 min and an alignment time window of 20 min. Carbamidomethyl cysteine was searched as a fixed modification. Oxidized methionine and protein N-term acetylation were set as variable modifications. Enzyme specificity was set as trypsin. The maximum missing cleavage site was set as 2. The tolerances of first search and main search for peptides were set at 20 ppm and 4.5 ppm, respectively. The minimal peptide length was set at 7. False discovery rates (FDRs) of peptide and protein were set with the cutoffs not greater than 1%.

LFQ intensity was used for proteomic data analysis. All analysis steps were conducted in Persus and R softwares. Missing values were imputed by method of normal distribution imputation in Perseus. Principal component analysis (PCA) was conducted using *factoextra* package in R. Differently expressed proteins were analyzed using a global permutation-based FDR approach implemented in Perseus. GO biological process enrichment analysis was performed using Fisher's exact test in Perseus.

Immunoblot analysis

The MCF7 cells were harvested with RIPA (P00013C, Beyotime, China) lysis buffer sitting on the ice after treated with 0.1% DMSO, 0.1 μM Geldanamycin or 35 μM **SOMCL-16-175** for 48 h. The cell debris was removed by centrifugation at 12000 rpm for 15 min, and the supernatant was collected. Protein concentrations for all of the samples submitted to western blot analysis were measured by using the Bradford method (Bradford kit, P0006C, Beyotime, China), and samples containing equal amounts of total protein were loaded for SDS-PAGE gel electrophoresis. The protein samples in polyacrylamide gel were then transferred onto 0.22 μM PVDF membrane (Millipore, United States) under a constant current running for 3 h. The membranes were blocked by using 5% defatted milk and incubated with primary antibodies (CDK1, CDK2, CDK4, Hsp70, Hsp90 and β-actin) in 4 ℃ for 16 h. After removing the primary antibodies, the membranes were further incubated with the secondary antibody (HRP-conjugated anti-mouse or HRP-conjugated anti-rabbit antibody) at room temperature for 2 h. Finally, chemiluminescent HRP substrate was applied to visualize specific proteins in the

membrane.

References

Adams, P.D., Grosse-Kunstleve, R.W., Hung, L.W., Ioerger, T.R., McCoy, A.J., Moriarty, N.W., Read, R.J., Sacchettini, J.C., Sauter, N.K., and Terwilliger, T.C. (2002). PHENIX: building new software for automated crystallographic structure determination. Acta Crystallogr D *58*, 1948-1954.

Bailey, S. (1994). The Ccp4 Suite - Programs for Protein Crystallography. Acta Crystallogr D *50*, 760-763.

Delaglio, F., Grzesiek, S., Vuister, G.W., Zhu, G., Pfeifer, J., and Bax, A. (1995). NMRPipe: a multidimensional spectral processing system based on UNIX pipes. Journal of biomolecular NMR *6*, 277-293.

Emsley, P., and Cowtan, K. (2004). Coot: model-building tools for molecular graphics. Acta Crystallogr D *60*, 2126-2132.

Fielding, L. (2007). NMR methods for the determination of protein-ligand dissociation constants. Prog Nucl Mag Res Sp *51*, 219-242.

Freiburger, L., Sonntag, M., Hennig, J., Li, J., Zou, P.J., and Sattler, M. (2015). Efficient segmental isotope labeling of multi-domain proteins using Sortase A. Journal of biomolecular NMR *63*, 1-8.

Harder, E., Damm, W., Maple, J., Wu, C.J., Reboul, M., Xiang, J.Y., Wang, L.L., Lupyan, D., Dahlgren, M.K., Knight, J.L.*, et al.* (2016). OPLS3: A Force Field Providing Broad Coverage of Drug-like Small Molecules and Proteins. J Chem Theory Comput *12*, 281-296.

Keller, R.L.J. (2004). The Computer Aided Resonance Assignment Tutorial. Cantina Verlag.

Kneller, D.G., and Kuntz, I.D. (1993). Ucsf Sparky - an Nmr Display, Annotation And Assignment Tool. J Cell Biochem, 254-254.

Koldso, H., Severinsen, K., Tran, T.T., Celik, L., Jensen, H.H., Wiborg, O., Schiott, B., and Sinning, S. (2010). The Two Enantiomers of Citalopram Bind to the Human Serotonin Transporter in Reversed Orientations. J Am Chem Soc *132*, 1311-1322.

Meyer, P., Prodromou, C., Hu, B., Vaughan, C., Roe, S.M., Panaretou, B., Piper, P.W., and Pearl, L.H. (2003). Structural and functional analysis of the middle segment of Hsp90: Implications for ATP hydrolysis and client protein and cochaperone interactions. Molecular cell *11*, 647-658.

Minor, W., Cymborowski, M., Otwinowski, Z., and Chruszcz, M. (2006). HKL-3000: the integration of data reduction and structure solution--from diffraction images to an initial model

in minutes. Acta crystallographica Section D, Biological crystallography *62*, 859-866.

Molina, D.M., Jafari, R., Ignatushchenko, M., Seki, T., Larsson, E.A., Dan, C., Sreekumar, L., Cao, Y.H., and Nordlund, P. (2013). Monitoring Drug Target Engagement in Cells and Tissues Using the Cellular Thermal Shift Assay. Science *341*, 84-87.

Sastry, G.M., Adzhigirey, M., Day, T., Annabhimoju, R., and Sherman, W. (2013). Protein and ligand preparation: parameters, protocols, and influence on virtual screening enrichments. J Comput Aid Mol Des *27*, 221-234.

Wang, Q.S., Zhang, K.H., Cui, Y., Wang, Z.J., Pan, Q.Y., Liu, K., Sun, B., Zhou, H., Li, M.J., Xu, Q*., et al.* (2018). Upgrade of macromolecular crystallography beamline BL17U1 at SSRF. Nucl Sci Tech *29*.

Yu, J.L., Chen, T.T., Zhou, C., Lian, F.L., Tang, X.L., Wen, Y., Shen, J.K., Xu, Y.C., Xiong, B., and Zhang, N.X. (2016). NMR-based platform for fragment-based lead discovery used in screening BRD4-targeted compounds. Acta pharmacologica Sinica *37*, 984-993.